Published October 24, 2016

Scramblase TMEM16F terminates T cell receptor signaling to restrict T cell exhaustion

Yu Hu,[1]* Ji Hyung Kim,[1]* Kangmin He,[2] Qi Wan,[1] Jessica Kim,[1] Melanie Flach,[1] Tom Kirchhausen,[2] Andrea Vortkamp,[3] and Florian Winau[1]

[1]Program in Cellular and Molecular Medicine, Boston Children's Hospital, Department of Microbiology and Immunobiology and [2]Program in Cellular and Molecular Medicine, Boston Children's Hospital, Department of Cell Biology, Harvard Medical School, Boston, MA 02115
[3]Department of Developmental Biology, University Duisburg-Essen, 45117 Essen, Germany

In chronic infection, T cells become hyporesponsive to antigenic stimulation to prevent immunopathology. Here, we show that TMEM16F is required to curb excessive T cell responses in chronic infection with virus. TMEM16F-deficient T cells are hyperactivated during the early phase of infection, exhibiting increased proliferation and cytokine production. Interestingly, this overactivation ultimately leads to severe T cell exhaustion and the inability of the host to control viral burden. Mechanistically, we identify TMEM16F as the dominant lipid scramblase in T lymphocytes that transports phospholipids across membranes. TMEM16F is located in late endosomes, where it facilitates the generation of multivesicular bodies for TCR degradation and signal termination. Consequently, TMEM16F deficiency results in sustained signaling and augmented T cell activation. Our results demonstrate that scramblase restricts TCR responses to avoid overactivation, ensuring a well-balanced immune response in chronic infectious disease.

INTRODUCTION

T cell activation is central to the adaptive immune response (Smith-Garvin et al., 2009). It occurs after recognition of MHC-bound peptides on APCs by the TCR. Activation of T lymphocytes is tightly regulated to acquire an appropriate immune response, as impaired T cell stimulation prevents the clearance of infectious pathogens (Zhang and Bevan, 2011). In contrast, persistent TCR triggering leads to the development of a unique state of T cells, known as exhaustion (Wherry, 2011). T cell exhaustion is found in chronic viral infections and tumors, in which T lymphocytes show compromised effector functions, as indicated by impaired cytokine production, high expression of inhibitory receptors, and reduced cytotoxic activity (Wherry, 2011).

The TCR is a multiprotein complex that is exclusively expressed on the surface of T lymphocytes (Hedrick et al., 1984; Yanagi et al., 1984). Upon antigen recognition, Src-family kinases, such as lymphocyte-specific protein tyrosine kinase (Lck), are activated and proceed to phosphorylate immunoreceptor tyrosine–based activation motifs (ITAMs) on the TCR-associated CD3 molecules. The phosphorylation of CD3 molecules, especially CD3ζ, creates docking sites for ζ-chain–associated protein kinase (ZAP) 70. Engagement of the tandem SH2 domain of ZAP70 by phosphorylated ITAMs therefore enables ZAP70 to activate and phosphorylate the key mediators of TCR signaling, such as linker for activation of T cells (LAT), which serves as a nucleation center for downstream signaling molecules.

The engagement of the TCR takes place at the conjunction between a T cell and an APC, known as the immunological synapse (IS). The IS is characterized by the segregation of membrane receptors and intracellular molecules into three ring-like structures: central supramolecular activation cluster (cSMAC), composed of TCR and protein kinase C (PKC) θ; peripheral SMAC, formed by lymphocyte function-associated antigen 1; and distal SMAC, rich in actin and CD45 (Monks et al., 1998; Grakoui et al., 1999). Upon TCR engagement, signaling events are initially generated and propagated in TCR microclusters in the periphery of the synapse. Subsequently, the TCR microclusters are translocated to the cSMAC for termination of signaling, potentially via multivesicular body (MVB)–mediated lysosomal degradation of TCRs (Varma et al., 2006; Vardhana et al., 2010).

Protein–lipid interactions are important for the dynamics of the IS (Gagnon et al., 2012; Le Floc'h et al., 2013). Several studies indicate that anionic lipids, especially phosphatidylserine (PS), are involved in the binding of the cytoplasmic domain of CD3ε and CD3ζ to the cell membrane (Xu et al., 2008; Zhang et al., 2011), which in turn regulates their function. Likewise, many TCR downstream molecules, such as PKCθ and AKT (Melowic et al., 2007; Huang et al., 2011), rely on lipid binding for their full activation, highlight-

*Y. Hu and J.H. Kim contributed equally to this paper.

Correspondence to Florian Winau: florian.winau@childrens.harvard.edu

Abbreviations used: cSMAC, central supramolecular activation cluster; ERK, extracellular signal regulated kinase; ESCRT, endosomal sorting complex required for transport; ILV, intraluminal vesicle; IS, immunological synapse; LAT, linker for activation of T cells; LBPA, lysobisphosphatidic acid; LCMV, lymphocytic choriomeningitis virus; MVB, multivesicular body; TIRF, total internal reflection fluorescence; TMEM, transmembrane protein; ZAP, ζ-chain–associated protein.

The Rockefeller University Press $30.00
J. Exp. Med. 2016
https://doi.org/10.1084/jem.20160612

Published October 24, 2016

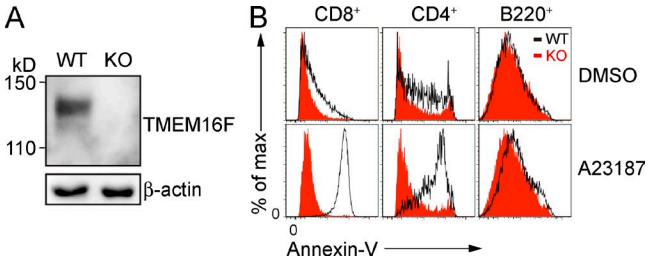

Figure 1. **TMEM16F is the dominant scramblase in T cells.** (A) Immunoblot analysis of TMEM16F expression in WT or TMEM16F-deficient (KO) thymocytes. (B) PS exposure was examined by Annexin V staining and flow cytometry on splenocytes from TMEM16F-KO or WT mice in response to calcium ionophore A23187. DMSO was used as control. B220, B cells. Data are representative of at least two independent experiments.

ing the possibility that altering lipid distribution affects T cell activation. Interestingly, antigen stimulation has been shown to trigger local changes of PS in TCR microclusters (Gagnon et al., 2012). However, the functional consequences of active lipid regulation with regard to T cell activation are unknown.

Lipid distribution is regulated by three types of lipid translocases: flippase, which translocates lipids from the outer to the inner leaflet of the cell membrane; floppase, which is an outwardly directed translocase; and scramblase, which is activated by Ca^{2+} and facilitates lipid transport across the membrane in a bidirectional fashion (Hankins et al., 2015). Flippase and floppase are mainly required for the ATP-dependent maintenance of asymmetric phospholipid distribution in membrane bilayers. With >90% of PS located in the inner leaflet of the membrane, it is unlikely that inactivation of these two lipid transporters induces rapid and robust redistribution of PS (Bevers and Williamson, 2010). Therefore, to study the active regulation of lipid redistribution, we focus our work on the well-defined lipid scramblase transmembrane protein (TMEM) 16F (Suzuki et al., 2010; Yang et al., 2012; Ehlen et al., 2013; Ousingsawat et al., 2015). TMEM16F, also called *Anoctamin 6*, was initially identified as a Ca^{2+}-dependent scramblase by expression cloning and shown to mediate lipid transport across membranes (Suzuki et al., 2010). Of note, Scott syndrome, an inherited bleeding disorder caused by defective phospholipid scramblase activity and lack of PS exposure on platelets (Weiss et al., 1979), was linked to loss-of-function mutations in the TMEM16F gene (Suzuki et al., 2010; Castoldi et al., 2011). Emerging evidence suggests that TMEM16F may have a dual function as Ca^{2+}-dependent phospholipid scramblase and Ca^{2+}-gated ion channel (Malvezzi et al., 2013; Brunner et al., 2014).

Here, we show that TMEM16F is the dominant scramblase in T cells and controls TCR-induced MVB formation. Moreover, we demonstrate that TMEM16F deficiency leads to an accumulation of activated TCRs and associated signaling molecules caused by impaired generation of MVBs. Remarkably, sustained TCR signaling causes severe exhaustion of T cells in chronic virus infection, which in turn leads to uncontrolled viral replication. These findings reveal a vital role of scramblase TMEM16F in termination of T cell activation, highlighting the importance of active lipid regulation to develop balanced immune responses.

RESULTS

TMEM16F is the dominant lipid scramblase in T cells

To test our hypothesis whether active regulation of lipid distribution controls the activation of T lymphocytes, we investi-

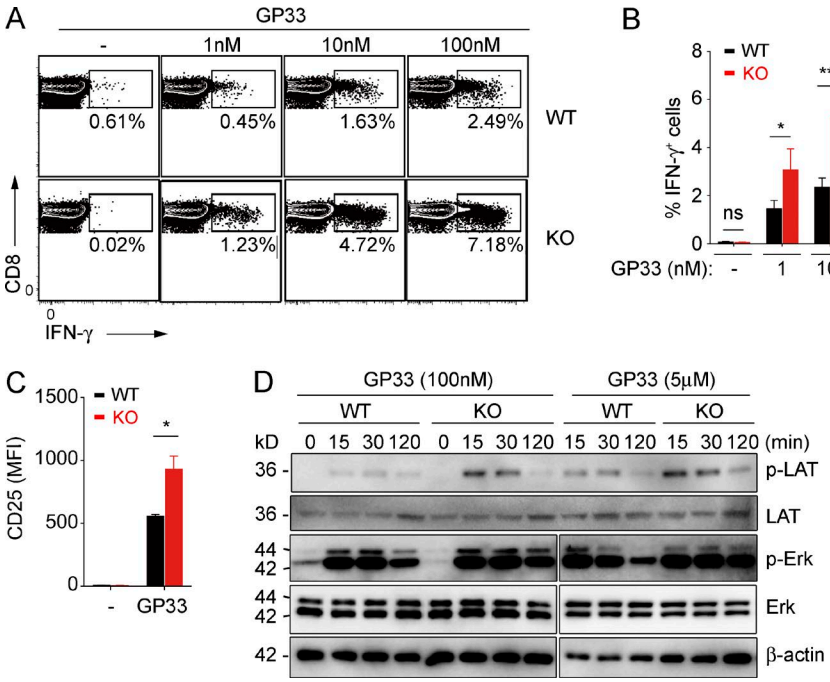

Figure 2. **Lack of TMEM16F causes increased T cell activation.** (A–C) Flow cytometry analysis of intracellular IFN-γ (A and B), and surface CD25 (C) of CD8 T cells activated by GP33. Quantification of IFN-γ–producing cells is shown in (B). MFI, mean fluorescence intensity. Results are displayed as mean ± SEM. *, $P < 0.05$; **, $P < 0.01$; ns, not significant, using Student's *t* test. B, $n = 6$; C, $n = 3$. (D) Phosphorylation of LAT and ERK induced by GP33 stimulation was detected by immunoblot of splenocytes from KO or WT mice. Data are representative of at least two experiments.

Published October 24, 2016

gated the impact of scramblase on T cell stimulation. First, we determined the expression of TMEM16F in T cells. Immunoblot data showed that thymocytes from WT mice expressed TMEM16F, whereas it was absent in TMEM16F-deficient cells (Fig. 1 A). To examine Ca^{2+}-dependent scramblase activity, we incubated lymphocytes with a calcium ionophore (A23187) to induce exposure of PS on the cell surface. We found that CD8 T cells lacking TMEM16F completely fail to scramble PS (Fig. 1 B). TMEM16F was also required for scrambling in CD4 T cells, although a minor subpopulation seemed to be TMEM16F-independent (Fig. 1 B). In contrast, TMEM16F did not facilitate PS exposure on B cells (Fig. 1 B). Thus, TMEM16F is the dominant scramblase in T lymphocytes.

Lack of TMEM16F amplifies T cell activation

Next, we investigated the effect of TMEM16F deficiency on T cell activation. To generate an antigen-specific system, we crossed TMEM16F-KO mice with P14-transgenic animals that express a TCR specific for glycoprotein GP33 from lymphocytic choriomeningitis virus (LCMV). After stimulation of splenocytes with an antigen, GP33 peptide, we observed that IFN-γ production by naive TMEM16F-deficient CD8 T cells was significantly increased (Fig. 2, A and B). Surface expression of the activation marker CD25 was similarly augmented on T cells lacking TMEM16F (Fig. 2 C). In parallel, we analyzed TCR downstream signaling to gain in-depth resolution of T cell stimulation. TMEM16F-deficient T cells showed stronger and sustained phosphorylation of LAT and ERK (extracellular signal regulated kinase), proximal and distal molecules in the TCR signaling cascade, respectively (Fig. 2 D). Notably, TMEM16F was not essential for the increase of intracellular calcium triggered by TCR stimulation (Fig. S1). Collectively, our data demonstrate that lack of TMEM16F causes increased T cell activation upon antigen stimulation.

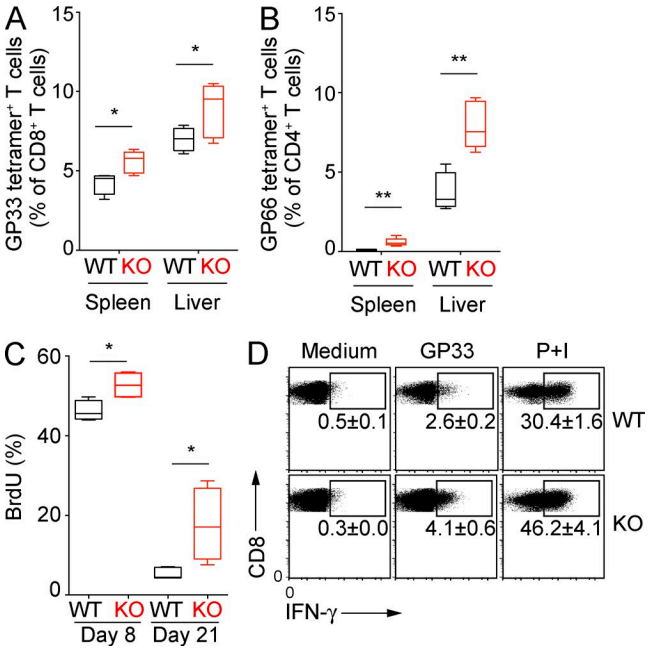

Figure 3. **Increased T cell activation in TMEM16F-KO mice during early phase of chronic infection.** (A–D) WT or TMEM16F-KO mice were i.v. infected with 4×10^6 pfu LCMV clone 13. T cell responses were analyzed on day 6 after infection (A, B, and D) and day 21 after infection (C). (A and B) Frequencies of GP33-tetramer–positive cells among total CD8 T cells in A, and GP66-tetramer–positive cells among total CD4 T cells in B were determined by flow cytometry. $n = 4$ for WT and $n = 5$ for KO. (C) Proliferation of GP33-tetramer–positive T cells from spleen was measured by BrdU incorporation at indicated time points after infection. $n = 4$, 4, 5, and 4, from left to right. (D) Flow cytometry analysis of intracellular IFN-γ production in CD8 T cells in response to GP33, or PMA and Ionomycin (P+I). $n = 4$ for WT; $n = 5$ for KO. Results are displayed as mean ± SEM of two independent experiments. *, $P < 0.05$; **, $P < 0.01$; ns, not significant, using Student's *t* test.

Increased T cell activation in TMEM16F-KO mice during early phase of chronic infection

Fine-tuning of T cell activation is crucial for effective immune responses. Persistent activation can lead to T cell exhaustion as seen in chronic viral infections (Wherry, 2011). Because we found sustained TCR signaling and over-activation of T cells in the absence of TMEM16F, we next addressed the disease relevance of this mechanism, namely the immune response and protection against chronic viral infection in TMEM16F-deficient animals. First, we excluded an effect of TMEM16F on T cell development. Numbers of CD8 and CD4 T cells in thymus and peripheral lymphatic organs, as well as frequencies of regulatory T (T reg) cells and iNKT cells, proved to be normal in TMEM16F-KO mice compared with WT littermate controls (Fig. S2). Next, we performed chronic infection with LCMV clone 13 and found increased frequencies of antigen-specific CD8 and CD4 T cells in TMEM16F-deficient mice within the first week after infection (Fig. 3, A and B). Increased activation of TMEM16F-deficient T cells was reflected by their augmented proliferation early after infection (Fig. 3 C). Although WT controls returned to background levels, T cells lacking TMEM16F remained highly proliferative at day 21 after infection (Fig. 3 C). In addition, T cells in TMEM16F-KO animals produced higher amounts of IFN-γ (Fig. 3 D). Increased T cell activation was not caused by an altered T reg cell compartment (Fig. S3) or expression of type I IFN (Fig. S4). In this study, we demonstrate that restriction of TCR signaling by TMEM16F prevents excessive T cell responses during the early phase of chronic infection.

TMEM16F deficiency causes severe T cell exhaustion

Because persistent T cell stimulation can lead to dysfunctional T cell responses, we subsequently examined T cell exhaustion at later stages of chronic infection. We found significantly increased expression of the exhaustion marker PD-1 on CD8 T cells from TMEM16F-deficient animals (Fig. 4, A and B). After stimulation with different CD8 T cell antigenic epitopes, coproduction of IFN-γ and TNF was strikingly decreased

Published October 24, 2016

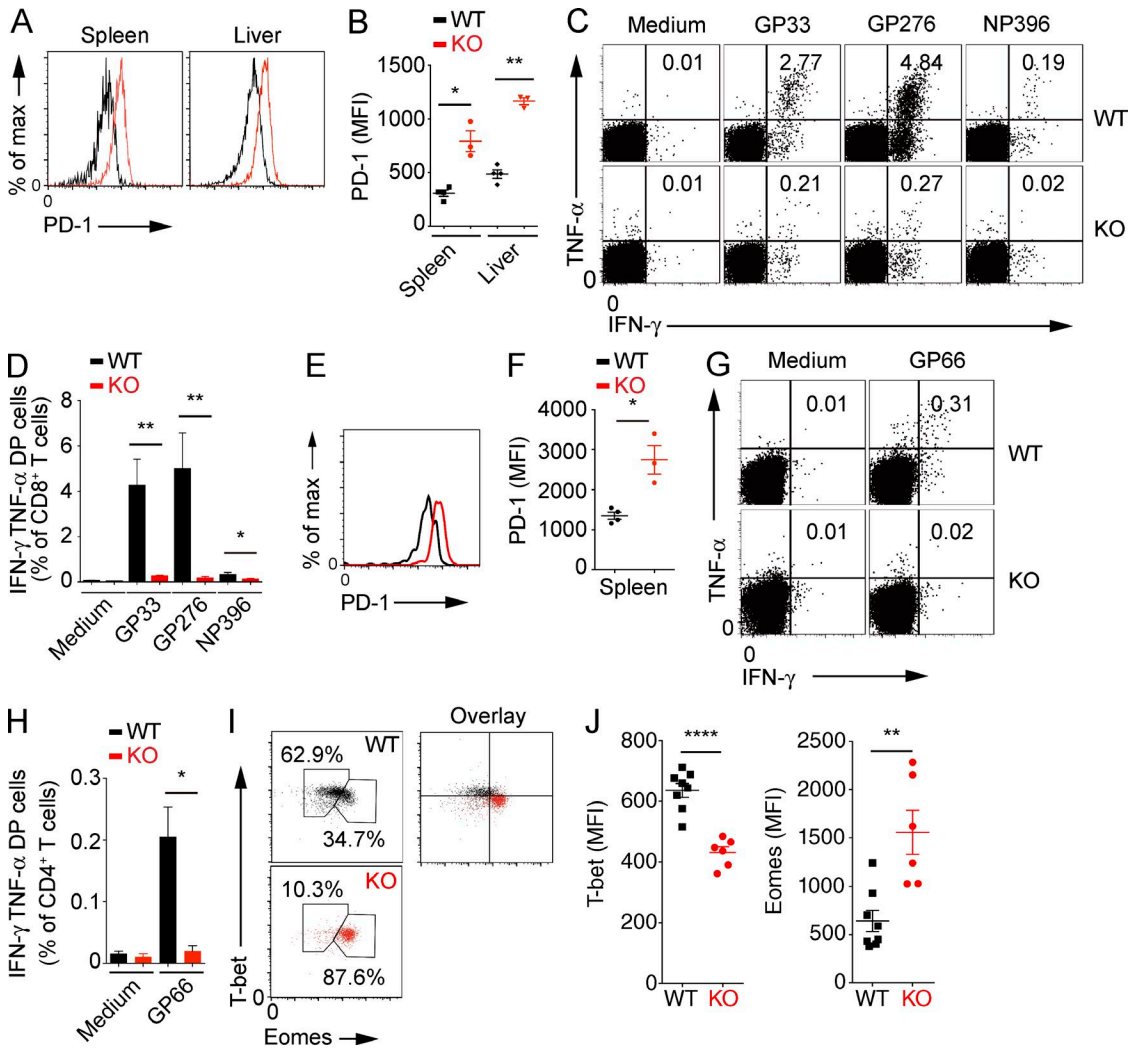

Figure 4. **TMEM16F deficiency causes severe T cell exhaustion.** (A–J) WT or TMEM16F-KO mice were i.v. infected with 4×10^6 pfu LCMV clone 13 for 80 d. (A–D) Expression of PD-1 in GP33-tetramer–positive CD8 T cells (A and B) and coproduction of IFN-γ and TNF in CD8 T cells from spleen after restimulation with indicated epitopes (C and D) were analyzed by flow cytometry. $n = 4$ for WT and $n = 3$ for KO. (E–H) Expression of PD-1 in GP66-tetramer–positive CD4 T cells (E and F) and coproduction of IFN-γ and TNF in CD4 T cells from spleen after restimulation with GP66 (G and H) were analyzed by flow cytometry. $n = 4$ for WT; $n = 3$ for KO. (I and J) Expression of T-bet and Eomes in GP33-tetramer–positive CD8 T cells were analyzed by flow cytometry. Data are pooled from two experiments. $n = 8$ for WT; $n = 6$ for KO. MFI, mean fluorescence intensity. Results are displayed as mean ± SEM of two to five independent experiments. Student's *t* test was used. *, $P < 0.05$; **, $P < 0.01$; ****, $P < 0.0001$.

when TMEM16F was lacking (Fig. 4, C and D). Similarly, antigen-specific CD4 T cells expressed higher amounts of PD-1, and produced less cytokines (Fig. 4, E–H). Thus, our data indicate that initial and sustained T cell overactivation causes severe T cell exhaustion in TMEM16F deficiency. In chronic LCMV infection, antiviral T cell responses are controlled and balanced by two T cell populations: T-bet^{hi} and Eomes^{hi} cells (Kao et al., 2011; Paley et al., 2012; Staron et al., 2014). T-bet^{hi} cells represent a pool of precursors, and Eomes^{hi} cells are a terminally differentiated population. As persistent antigenic stimulation is linked to the transition of T-bet^{hi} to Eomes^{hi} cells (Kao et al., 2011; Paley et al., 2012), TMEM16F deficiency may break the balance between those two populations to eventually deplete T-bet^{hi} cells. As anticipated, later in chronic infection, T-bet expression was diminished whereas Eomes was complementarily increased in TMEM16F-deficient cells, indicating terminal differentiation of T cells (Fig. 4, I and J). To confirm that TMEM16F acted directly in CD8 T cells, we generated BM chimera using *Rag1*$^{-/-}$ mice as recipients. Consistently, during chronic infection, TMEM16F-deficient CD8 T cells were severely exhausted (Fig. 5, A–C). This defect proved to be T cell–intrinsic, as TMEM16F-deficient CD8 T cells exclusively failed to produce cytokines compared with WT in chronic infection of mixed BM chimera (Fig. 5 D). Moreover, the T-bet^{hi} precursor pool was largely depleted when TMEM16F was lacking

Published October 24, 2016

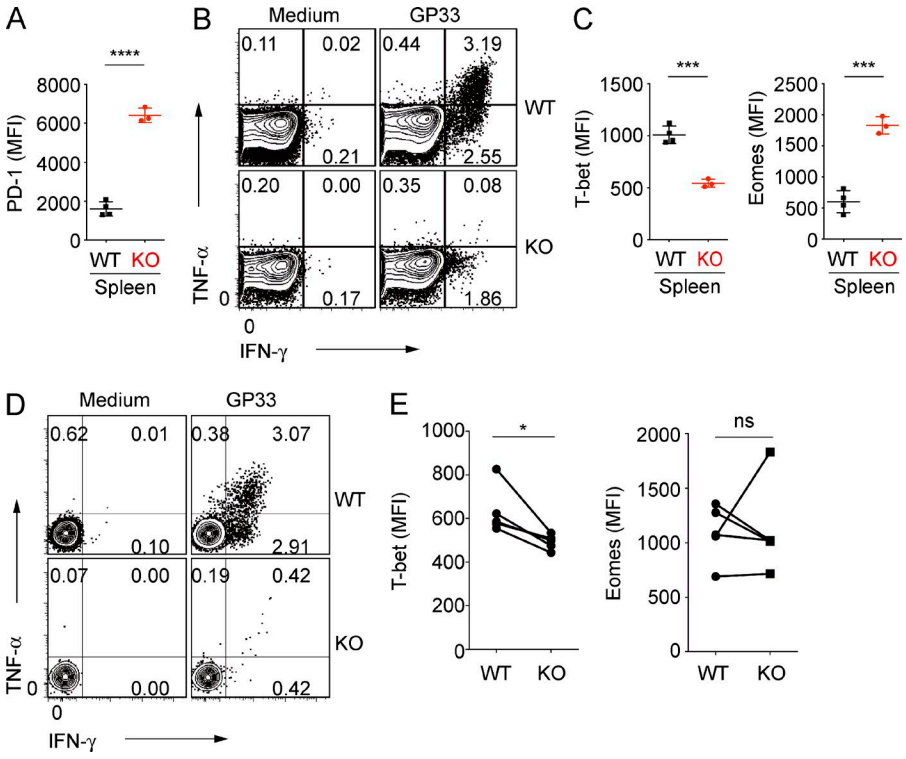

Figure 5. **TMEM16F regulates T cell response in a cell-intrinsic manner.** (A–C) WT or TMEM16F-deficient BM chimeric mice were i.v. infected with 4×10^6 pfu LCMV clone 13 and sacrificed at day 150 after infection. Expression of PD-1 (A) and T-bet and Eomes (C) in GP33-tetramer–positive CD8 T cells, and cytokine production in CD8 T cells after stimulation with GP33 (B) were analyzed by flow cytometry. $n = 4$ for WT; $n = 3$ for KO. (D and E) Mixed BM chimera were infected as in A–C. Mice were sacrificed at day 150 after infection. Cytokine production in WT or KO CD8 T cells after stimulation with GP33 in D, and expression of T-bet and Eomes in GP33-tetramer–positive CD8 T cells in E, were determined by flow cytometry. $n = 4$ for each group. MFI, mean fluorescence intensity. Results are displayed as mean ± SEM of at least two independent experiments. *, $P < 0.05$; ***, $P < 0.001$; ****, $P < 0.0001$; ns, not significant, using Student's *t* test.

(Fig. 5 E). Collectively, our results indicate that TMEM16F is vital to protecting T lymphocytes from severe exhaustion during chronic infection.

TMEM16F is required for control of chronic virus infection

Taking into account that the balance of T-bet^{hi} and Eomes^{hi} cell populations is vital to maintain the cytotoxic T lymphocyte (CTL) pool (Paley et al., 2012), we observed a reduced number of antigen-specific CD8 T cells in TMEM16F-KO mice (Fig. 6 A). Because it is well established that CD8 T cells are essential to control LCMV clone 13 infection, the impaired maintenance of the CTL pool in TMEM16F-KO mice suggests an insufficiency to resolve the infection. In WT mice, virus in blood and tissues, such as the liver, was cleared 2 mo after infection (Fig. 6 B). However, TMEM16F deficiency leads to uncontrolled viremia (Fig. 6 B), as well as failure of virus clearance in tissues (Fig. 6, C and D). Our results indicate that TMEM16F is critical to maintain a partial but effective antiviral T cell response to limit chronic virus infection.

TMEM16F is recruited to the IS and resides in late endosomes

To elucidate the molecular mechanism behind how TMEM16F controls T cell activation, we next tracked its cellular localization and function. To this end, T cells transduced with fluorescent TMEM16F were co-cultured with antigen-presenting B cells. After antigen stimulation, TMEM16F was recruited to the IS as revealed by confocal microscopy (Fig. 7 A). Of note, TMEM16F appeared mainly in intracellular structures instead of the plasma membrane (Fig. 7 A). To kinetically demonstrate the recruitment of TMEM16F to the TCR activation site, we used TIRF (total internal reflection fluorescence) microscopy to visualize membrane proximal events of T cells on stimulatory coverslips (Fig. 7, B and C; and Video 1). TMEM16F was found to be highly motile, with a velocity reaching up to 1.5 µm/s, a speed similar to vesicle trafficking (Video 1). To test the mechanics of TMEM16F-positive vesicle movement, we performed TIRF live imaging while modulating the functions of the cytoskeleton. Inhibition of actin–myosin contractions by blebbistatin did not alter recruitment of TMEM16F to the T cell activation site (Fig. 7, D and E; and Video 2). In contrast, treatment with nocodazole that disrupts the microtubule network reduced migration of TMEM16F vesicles, indicating the movement of TMEM16F was largely mediated by microtubules but not actin (Fig. 7, D and E; and Video 2). Therefore, to precisely define the subcellular compartment of TMEM16F, we assessed its co-localization with endosomal reporters in T cells, using image series taken from TIRF microscopy. Accordingly, Rab7 largely co-localized with TMEM16F, indicating that it mainly resides in late endosomes (Fig. 8 A and Video 3). As controls, TMEM16F did not co-localize with the early endosomal marker Rab5 (Fig. 8 B and Video 4), or with Rab11, which labels recycling endosomes (Fig. 8 C and Video 5). Moreover, the localization of TMEM16F in a Rab7-positive compartment was independent of T cell activation status (Fig. 8 D). However, the abundance of TMEM16F in late endosomes increased upon TCR triggering (Fig. 8 D). In all, these find-

Published October 24, 2016

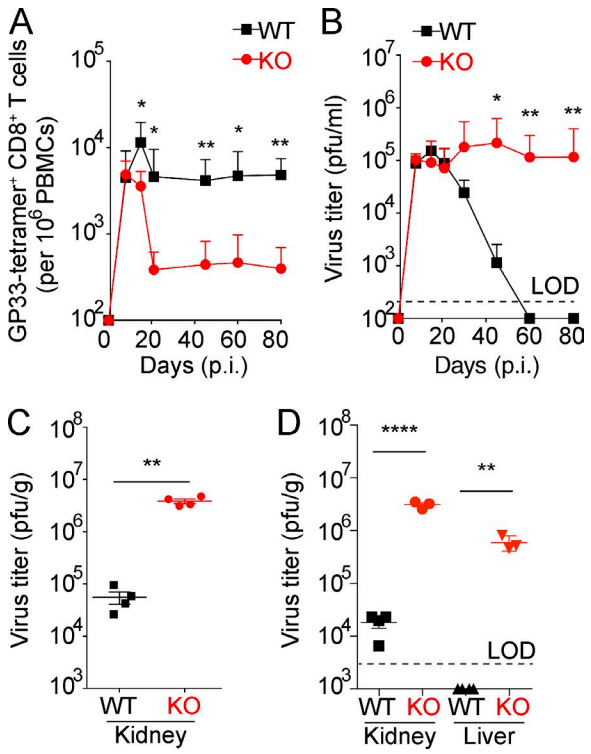

Figure 6. **TMEM16F is required for control of chronic viral infection.** (A–C) WT or TMEM16F-KO mice were i.v. infected with 4×10^6 pfu LCMV clone 13 for 80 d (A and B) or 150 d (C). (A) Absolute number of GP33-tetramer–positive CD8 T cells per 10^6 PBMCs was analyzed by flow cytometry at indicated time points after infection. $n = 4$ for WT; $n = 3$ for KO. (B and C) Virus loads in serum in B at indicated time points and in kidney at 138 d after infection in C were determined by focus assay. (B) $n = 4$ for WT $n = 3$ for KO; (C) $n = 4$. (D) WT or TMEM16F-deficient BM chimeric mice were i.v. infected with 4×10^6 pfu LCMV clone 13 and sacrificed at day 150 after infection. Virus loads in kidney and liver of BM chimeric mice were determined by focus assay. LOD, limit of detection. $n = 4$ for WT; $n = 3$ for KO. Results are displayed as mean ± SEM of two to three independent experiments. Student's *t* test was used. *, $P < 0.05$; **, $P < 0.01$; ****, $P < 0.0001$.

ings reveal an unexpected localization of TMEM16F in late endosomes, pointing to the existence of an unidentified endosomal mechanism for TCR signal termination.

TMEM16F is involved in MVB formation upon TCR engagement

Late endosomes are also known as MVBs, which are unique compartments that contain intraluminal vesicles (ILVs). The major role of MVBs is to degrade their contents via fusion with lysosomes. In T cells, MVBs have been associated with TCR degradation and signal termination (Varma et al., 2006; Vardhana et al., 2010). To address the impact of TMEM16F on MVB formation, we performed stainings for lysobisphosphatidic acid (LBPA), a marker for ILVs (Kobayashi et al., 1998). Interestingly, stimulation through the TCR greatly increased the number of LBPA-positive vesicles in T cells (Fig. 9, A and B), indicating that TCR signaling enhances MVB formation. To evaluate whether TMEM16F is involved in this process, we performed knockdown of TMEM16F in T cells using shRNA. Lack of TMEM16F had no impact on the amount of LBPA-containing vesicles in unstimulated T cells, however, after TCR stimulation, the increase in LBPA-positive vesicles in controls was abrogated in TMEM16F-silenced T cells (Fig. 9 C). Because the occurrence of ILVs in endosomes defines MVBs, we subsequently investigated the ultrastructure of the endosomal compartment in T cells lacking TMEM16F. Analysis by electron microscopy revealed a significantly reduced number of ILVs per MVB in TMEM16F-deficient T cells (Fig. 9, D and E). After a classification of different MVB maturation stages (Vogel et al., 2015), we found that MVB1, characterized by electron-translucent lumen and ≤3 ILVs, was strikingly more abundant in the absence of TMEM16F (Fig. 9 F). Consequently, MVB2 (translucent lumen, >3 ILVs) and especially mature MVB3 (stained vacuole, >3 ILVs) were less numerous in TMEM16F-deficient T cells (Fig. 9 F), showing that a defect in TMEM16F delays the progression of MVB development. Collectively, these data demonstrate that TMEM16F is involved in the increased generation of MVBs upon T cell activation.

Impaired cSMAC formation and sustained TCR signaling in TMEM16F-deficient T cells

Because functional MVBs are involved in the development of the IS center where TCRs accumulate for signal termination (Varma et al., 2006; Vardhana et al., 2010), we next investigated the impact of TMEM16F on cSMAC formation. Confocal microscopy, followed by 3D reconstruction of the contact site between antigen-presenting B cells and responding T cells was performed to visualize the IS en face (Fig. 10, A and B). In control cells, the cSMAC formed as a dense spot of TCRs. In contrast, in TMEM16F-deficient T cells, TCRs remained in the periphery and failed to translocate to the IS center (Fig. 10 A). A defect in cSMAC formation has been shown to cause chronic TCR signaling (Vardhana et al., 2010). Thus, to functionally detect active TCR signaling, we transduced T cells with the SH2 domain of ZAP70 that specifically binds to phosphorylated tyrosine residues in the CD3 signaling units of TCRs (Yudushkin and Vale, 2010). Using real-time TIRF microscopy, we demonstrate that active TCR signaling is sustained in TMEM16F-deficient T cells (Fig. 10, C and D; and Video 6). To further evaluate key events in TCR signal transduction, we examined the dynamics of LAT microclusters at the TCR activation site. Notably, dissolution of these microclusters indicates signal termination. In accordance with our findings of increased LAT phosphorylation in T cells lacking TMEM16F (Fig. 2 D), live imaging revealed an increase of newly formed LAT microclusters in TMEM16F-deficient T cells (Fig. 10, E and F; Video 7). Moreover, whereas LAT microclusters subsided in control cells minutes after T cell activation, they were stable over time in T cells deficient for TMEM16F (Fig. 10, E and F; and Video 7). Together, these results reveal that TMEM16F is important in termi-

Published October 24, 2016

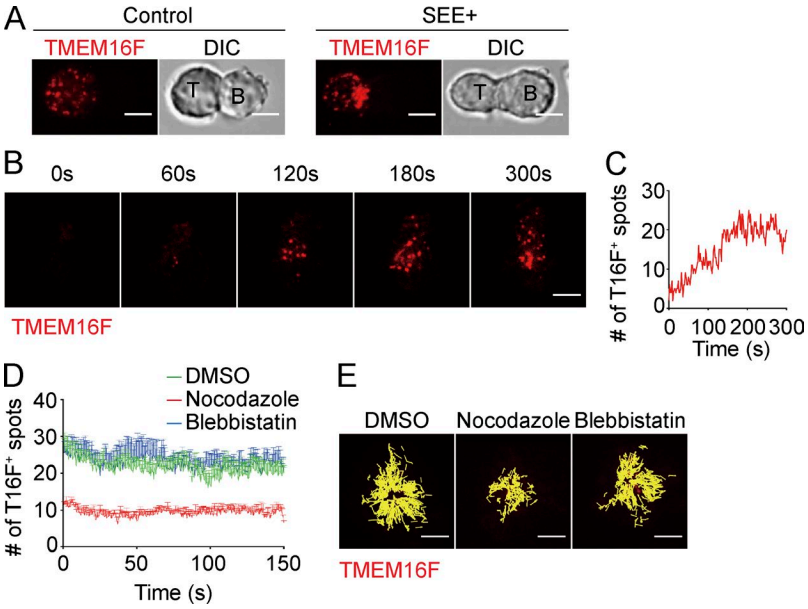

Figure 7. **TMEM16F is recruited to the synapse and requires microtubules for transport.** (A–E) Jurkat cells expressing TMEM16F-RFP were co-cultured with Raji cells (A) or stimulated on coverslips coated with αCD3 (B–E). (A) Confocal microscopy analysis for localization of TMEM16F in Jurkat T cells co-cultured with control (unpulsed) or SEE-pulsed Raji B cells (SEE$^+$). 2-µm z stack of images is shown. DIC, differential interference contrast. (B and C) Dynamics of TMEM16F at the TCR activation site were imaged by TIRF microscopy. Number of TMEM16F-positive spots was quantified in C. (D and E) Dynamics of TMEM16F at the TCR activation site were imaged by TIRF microscopy in Jurkat cells pretreated with vehicle (DMSO), 1 µM nocodazole, or 1 µM blebbistatin. (D) Number of TMEM16F-positive spots was quantified. Time zero is the start of recording. $n = 5$ for each group. (E) Trajectories of TMEM16F-positive spots were tracked by ImageJ. Bars, 5 µm. Data are representative of three independent experiments.

nating TCR signaling by promoting cSMAC formation and subsequent degradation of active TCRs and associated signaling molecules.

DISCUSSION

Our work presents a novel mechanism to terminate TCR signaling by lipid scramblase TMEM16F. We propose that TCR engagement, via increased intracellular Ca^{2+} levels, activates scramblase TMEM16F in late endosomes to mediate the formation of MVBs. Newly generated MVBs sequester intracellular TCR signaling complexes for subsequent lysosomal degradation to terminate T cell activation. This TMEM16F-mediated checkpoint determines the duration of signaling and the proper ratio of T-bet^{hi} to Eomes^{hi} effector T cells to facilitate virus clearance. In the absence of TMEM16F, generation of MVBs is hampered, TCR signaling molecules accumulate, and T cell activation is sustained. Breaking the TMEM16F checkpoint leads to prolonged signaling that shifts the balance toward terminally differentiated Eomes^{hi} T cells and ultimate loss of virus protection (Fig. S5).

We identified an unexpected localization of TMEM16F in endocytic compartments of T cells, which will provide novel mechanistic insights into endosomal lipid regulation and its functional consequences for cell signaling. Accordingly, regulation of PS exposure was thought to be restricted to the plasma membrane. Based on our findings, endosomes may be used as an extra pool, providing PS for accumulation on the outer leaflet of the plasma membrane. Indeed, previous studies have shown that calcium-mediated endosomal trafficking contributes to PS exposure upon apoptosis induction (Lee et al., 2013). However, because TMEM16F is dispensable for PS exposure during apoptosis (Segawa et al., 2014), the contributions of the endosomal pool to TMEM16F-dependent PS exposure remain to be evaluated.

Increasing evidence indicates that endosomes are not simply recipients of internalized receptors, but also sorting stations for either their degradation in lysosomes, or recycling to the plasma membrane, respectively (Irannejad et al., 2015). The balance between degradation and recycling dictates the outcome of signals initiated at the plasma membrane with regard to the quality of elicited responses, such as cell proliferation and survival. Furthermore, endosomes also serve as physical platform for signal transduction (Pálfy et al., 2012). For example, endosomal epidermal growth factor receptors (EGFRs) contribute significantly to the overall EGFR signaling capacity (Fortian and Sorkin, 2014). Moreover, endosomes in T cells contain several key TCR signaling molecules (Benzing et al., 2013), whose activities are important for sustained TCR signaling and cell growth (Yudushkin and Vale, 2010; Willinger et al., 2015). Therefore, an important question is how endosomal signaling is terminated (Irannejad et al., 2015). One well-established mechanism is by sorting of activated receptor complexes into MVBs, mainly mediated by the endosomal sorting complex required for transport (ESCRT). In addition to ESCRT, collective evidence indicates that lipids also play key roles in MVB generation. For example, LBPA and ceramide induce membrane bending to promote formation of ILVs (Matsuo et al., 2004; Trajkovic et al., 2008). Interestingly, we found that the level of LBPA is increased upon TCR stimulation, which is correlated with the elevated number of MVBs in activated T cells that we identified by electron microscopy. Furthermore, our work shows that lack of TMEM16F greatly reduces LBPA abundance only in activated T cells but not in resting cells, emphasizing an actively regulated process mediated by TMEM16F. However, it is not known if LBPA is the only driving force for ILV generation or whether it needs the cooperation of other lipids or proteins. A previous study using liposome assays showed that lipid

Published October 24, 2016

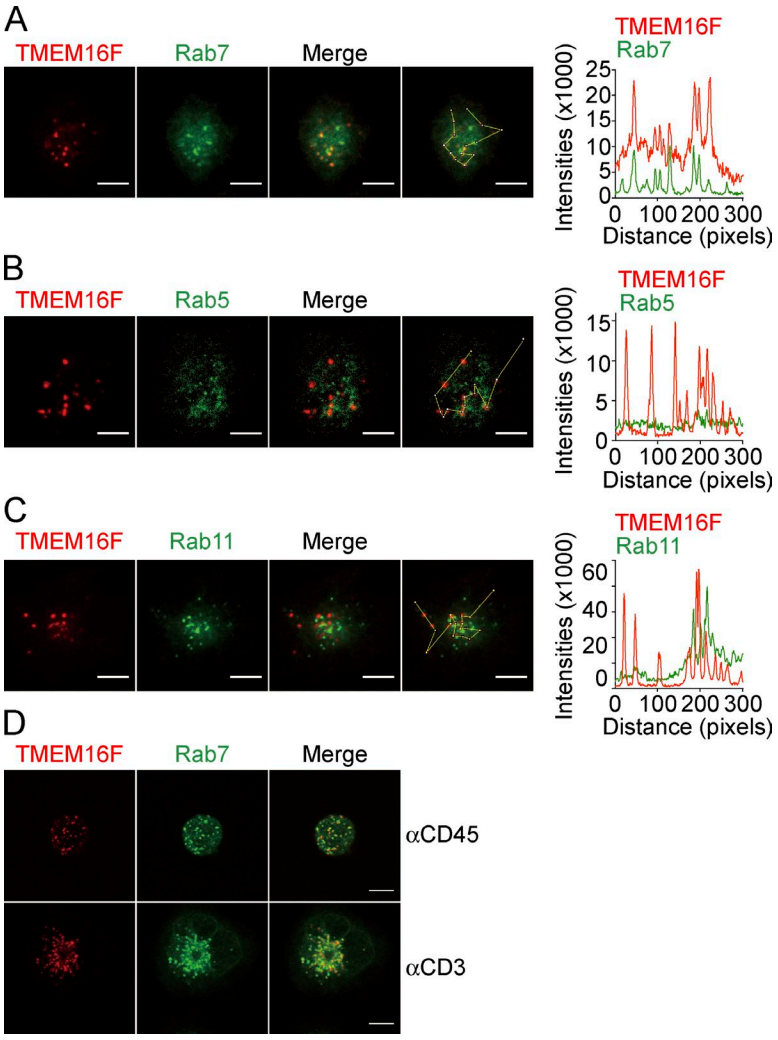

Figure 8. **TMEM16F resides in late but not early or recycling endosomes.** (A–D) Jurkat cells expressing TMEM16F-RFP together with Rab7-GFP (A and D), Rab5-GFP (B), and Rab11-GFP (C) were stimulated on coverslips coated with αCD45 (D) or αCD3 (A–D). Cells were imaged by TIRF (A–C) or confocal microscopy (D). (A–C) Spatial correlation of localization of TMEM16F and Rab7 (A), Rab5 (B), or Rab11 (C) upon TCR stimulation. The fluorescence intensities (pixels) along the dotted line were determined by ImageJ (right). Images are representative of six to seven cells. Bars, 5 µm.

composition affects the efficiency of ESCRT-mediated membrane scission during ILV generation (Wollert et al., 2009), indicating that ESCRT and locally enriched lipids might cooperatively control MVB formation. In addition, asymmetric distribution of lipids generates curvature during endosome trafficking and autophagosome formation (Hailey et al., 2010; Xu et al., 2013), a principle that can be applied to ILV generation as well. Collectively, we propose that TMEM16F might locally regulate lipid redistribution in the endosomal membrane, which is able to modify the biophysical properties of the membrane for subsequent deformation (Stachowiak et al., 2013). In this context, we show that in the absence of TMEM16F, de novo generation of ILVs and MVBs is hampered, leading to accumulation of TCR signaling molecules and T cell activation that proceeds without restraint (Fig. S5).

Lastly, we demonstrate that TMEM16F functions as an essential factor to restrict persistent infection with virus. It is known that continuous antigenic stimulation suppresses T cell activation in chronic viral infection (Staron et al., 2014). Our work reveals that TMEM16F plays a critical role in this process, as TMEM16F-deficient T cells are not able to curb proliferation in vivo. In addition, suppression of T cell responses during chronic viral infection was shown to protect the host from immunopathology (Ou et al., 2008). Surprisingly, overactivation of T cells in TMEM16F deficiency does not affect mortality, but instead results in severe T cell exhaustion and defective antiviral responses, highlighting the sophisticated control of T cell responses in vivo. Significant advances have been made recently to better understand T cell exhaustion. It is commonly accepted that exhausted CD8 T cells still retain partial effector functions, which are crucial to restrain viral infection (Paley et al., 2012; Staron et al., 2014). In particular, the presence of T-bet^{hi} precursors in the exhausted population enables effective immunotherapy, owing to the fact that mainly T-bet^{hi} cells have the potential for reinvigoration after PD-1 pathway blockade (Blackburn et al., 2008). Remarkably, the presence of TMEM16F is a prerequisite for the maintenance of T-bet^{hi} cells during chronic infection, introducing TMEM16F as novel immune checkpoint to allow for a well-balanced immune response

Published October 24, 2016

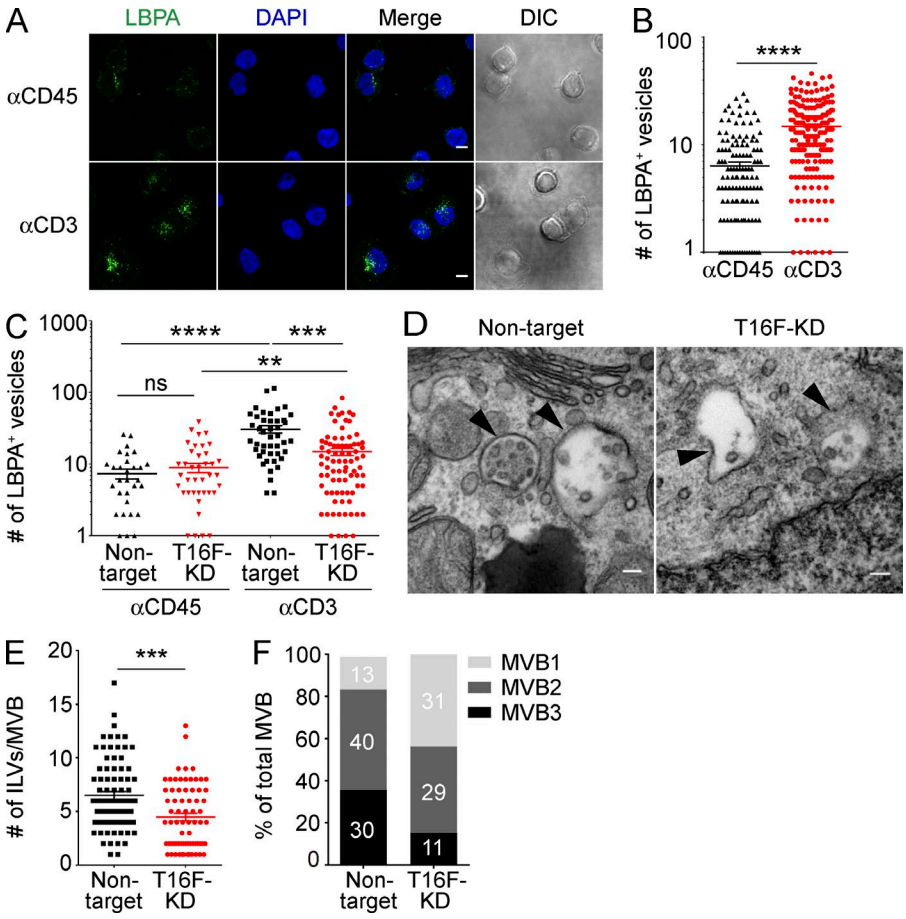

Figure 9. **TMEM16F is involved in MVB formation upon TCR engagement.** (A and B) Confocal microscopy analysis of LBPA staining of Jurkat cells seeded on coverslips coated with αCD45 (nonstimulatory) or αCD3 (stimulatory). 2-µm z stack of images is shown. Representative images are shown in A. Number of LBPA-positive vesicles was quantified in (B). Bars, 5 µm. DIC, differential interference contrast. n = 142 for αCD45; n = 190 for αCD3. (C) Quantification of LBPA-positive vesicles in nontarget (control) or T16F-KD (TMEM16F-knockdown) Jurkat T cells treated with αCD45 or αCD3. n = 33, 44, 44, and 85, from left to right. (D–F) Electron microscopy of MVBs in nontarget or T16F-KD Jurkat T cells. Representative electron micrographs are shown in D. Arrows indicate MVBs. Bars, 100 nm. Quantification of the number of ILVs per MVB and categorization of MVB stages are shown in E and F, respectively. n = 83 for nontarget and n = 71 for T16F-KD. Results are displayed as mean ± SEM. **, $P < 0.01$; ***, $P < 0.001$; ****, $P < 0.0001$; ns, not significant, using Student's t test. Data are representative of three experiments.

(Fig. S5). Ultimately, we propose targeting of TMEM16F to enhance its function to avoid exhaustion or reinvigorate T cell responses, thus enabling therapeutic strategies to improve efficacy of anti–PD-1 treatment against chronic diseases such as viral infection or cancer.

MATERIALS AND METHODS

Mice

Generation of *TMEM16F*$^{-/-}$ mice has been reported previously (Ehlen et al., 2013). WT littermate mice were used as control. WT and *TMEM16F*$^{-/-}$ mice were crossed to P14 TCR-transgenic animals. P14 TCR-transgenic mice were a gift from U. von Andrian (Harvard Medical School, Boston, MA). *Rag1*$^{-/-}$ mice were purchased from the The Jackson Laboratory. All animal procedures were approved by the Institutional Animal Care and Use Committee at Harvard Medical School.

Cells

MC57G and Jurkat cells (clone E6-1) were obtained from ATCC. Raji cells and 293T cells were provided by J. Lieberman (Boston Children's Hospital, Boston, MA), and N. Hacohen (Massachusetts General Hospital, Boston, MA), respectively. Raji and Jurkat cells were cultured in RPMI-1640 supplemented with 10% FBS, 2 mM L-glutamine, 50 µM β-mercaptoethanol (β-ME), 10 U/ml penicillin/streptomycin, 1 mM sodium pyruvate, and 100 mM Hepes. MC57G and 293T cells were cultured in Dulbecco's modified Eagle's medium supplemented with 10% FBS, 2 mM L-glutamine, 10 U/ml penicillin and streptomycin, and 1 mM sodium pyruvate. All cell culture reagents were obtained from Life Technologies unless otherwise noted.

Plasmids

PMX-TMEM16F-RFP was provided by S. Nagata (Kyoto University, Kyoto, Japan). TMEM16F-RFP fusion cDNA was subcloned into pHAGE2 lentiviral vector under control of the tetracycline-responsive element (TRE) promoter (a gift from D. Rossi, Boston Children's Hospital, Boston, MA). This vector harbors a human NGFR reporter separated by a P2A peptide fused in-frame upstream of TMEM16F-RFP. LAT-YFP was a gift from L.E. Samelson (National Institutes of Health [NIH], Bethesda, MD). PHR-mCherry-tSH2 (ZAP70), GFP-Rab5, GFP-Rab7, and GFP-Rab11 were obtained from Addgene. PLKO.1-Thy1.1 was provided by K. Wucherpfennig (Dana Farber Cancer Institute, Boston, MA). shRNA hairpin (TRCN0000134710) for human TMEM16F was obtained from the Sigma Mission library (Sigma-Aldrich).

Published October 24, 2016

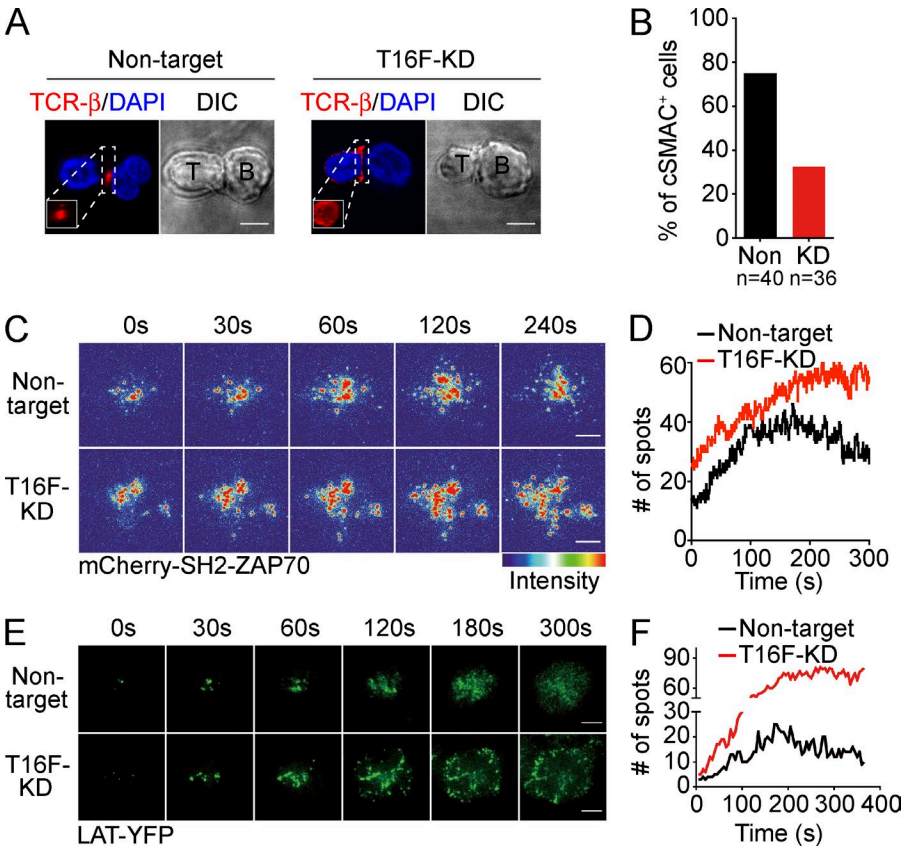

Figure 10. **Impaired cSMAC formation and sustained TCR signaling in TMEM16F-silenced T cells.** (A and B) Confocal microscopy analysis of cSMAC formation by measuring centralized accumulation of TCR-β at the IS between Jurkat T cells and SEE-pulsed Raji B cells. Percentage of cSMAC-positive cells is shown in B. Insets are 3D reconstructions of the IS en face. Non, control; KD, TMEM16F-knockdown. DIC, differential interference contrast. (C and D) Nontarget or T16F-KD Jurkat cells expressing mCherry-tSH2-ZAP70 were stimulated on αCD3-coated coverslips. Dynamics of mCherry-tSH2-ZAP70 at the TCR activation site were imaged by TIRF microscopy. SH2 domain of ZAP70 specifically binds to phosphorylated tyrosine residues in the CD3 signaling units of TCRs. Signal from the phosphotyrosine probe is depicted as thermal intensity in C. Number of mCherry-tSH2-ZAP70–positive spots were quantified in D. (E and F) Dynamics of LAT microclusters at the TCR activation site were imaged by TIRF microscopy. Number of LAT microclusters is quantified in F. Bars, 5 µm. Data are representative of three experiments.

Nontarget shRNA hairpin was used as a negative control (SHC002; Sigma-Aldrich). shRNA hairpins were subcloned into pLKO-Thy1.1 lentiviral vector using BamHI and NdeI.

PS exposure

PS exposure assay was performed as previously reported (Suzuki et al., 2010). In brief, cells were treated with 1 µM A23187 (Sigma-Aldrich) in Ca^{2+}-free HBSS buffer (Life Technologies) at 37°C for 15 min. After washing once with ice-cold HBSS buffer, cells were stained with FITC-Annexin V (eBioscience) together with fluorochrome-conjugated antibodies on ice for 15 min. Cells were washed and analyzed by flow cytometry.

Flow cytometry

The following antibodies were used for flow cytometry: CD8 (cat. no. 553035), B220 (553088), CD44 (553133), CD3ε (553066), and CD25 (102012) were purchased from BD; CD4 (cat. no. 100531), CD8 (100705), IFN-γ (505826), IL-2 (503808), T-bet (644808), Thy1.1 (202508), PD-1 (109109), CD45.1 (110722), and human NGFR (345108) were obtained from BioLegend; PD-1 (cat. no. 50–2073-82), FoxP3 (12-5773-82), TNF (17-7321-81), and Eomes (51-4875-82) were purchased from eBioscience.

Viability dye (eBioscience) or propidium iodide (PI; Sigma-Aldrich) were used in all experiments to exclude dead cells. For surface antigens, cells were stained with antibody cocktail in FACS buffer (PBS containing 0.5% BSA) on ice for 30 min. For intracellular cytokine staining, cells were stimulated with antigen or PMA (50 ng/ml) and Ionomycin (500 ng/ml; Sigma-Aldrich) for 3–5 h in the presence of GolgiStop (BD) before surface antigen staining. Next, cells were fixed and stained for cytokines using Cytofix/Cytoperm kit (BD) according to the manufacturer's protocol. Staining of FoxP3, T-bet, and Eomes was performed using Foxp3/Transcription Factor Staining Buffer set (eBioscience) per the manufacturer's instructions. Cells were processed using FACSCanto II (BD). All flow cytometry data were analyzed with FlowJo (Tree Star).

Immunoblot

Cells were lysed in loading buffer (62.5 mM Tris-HCl, 2% [wt/vol] SDS, 10% glycerol, and 0.01% β-ME [wt/vol]). For phosphorylation analysis, 10^6 splenocytes from P14-WT or P14-*TMEM16F*$^{-/-}$ mice were stimulated with GP33 for indicated time periods. Stimulation was terminated by adding 2× loading buffer (125 mM Tris-HCl, 4% [wt/vol] SDS, 20% glycerol, and 0.02% β-ME [wt/vol]). After boiling for 5 min, whole-cell lysates were separated via SDS-PAGE, transferred to nitrocellulose membrane (Bio-Rad Laboratories), and stained with primary antibodies, followed by HRP-labeled anti–mouse IgG (Santa Cruz Biotechnology, Inc.) or anti–rab-

Published October 24, 2016

bit IgG (ab6721; Abcam), and then visualized with SuperSignal West Pico Chemiluminescent Substrate (Thermo Fisher Scientific). To detect TMEM16F expression, lysate from the same number of WT or *TMEM16F*$^{-/-}$ thymocytes was used for loading. Antibody for TMEM16F was kindly provided by Lily Jan (University of California, San Francisco, San Francisco, California; Yang et al., 2012). Antibodies used in the experiments were: phospho-LAT (07–278; Merck Millipore), LAT (sc-7948; Santa Cruz Biotechnology, Inc.), phospho-Erk1/2 (4377; Cell Signaling Technology), Erk1/2 (C4695; Cell Signaling Technology), and β-actin (ab8227; Abcam).

Calcium flux assay

Splenocytes were stained with Ca^{2+} indicator dyes Fura Red and Fluo-4, stained for CD4 and CD8, and resuspended in serum-free RPMI. EGTA (0.5 mM) was added to cell suspensions to chelate extracellular Ca^{2+} in RPMI (0.4 mM Ca^{2+}). Splenocytes prestained with biotinylated anti-CD3 (5 µg/ml) were treated with streptavidin (20 µg/ml), followed by $CaCl_2$. Intracellular Ca^{2+} amounts were shown as a median ratio of Fluo-4/Fura Red over time.

TIRF microscopy

Sample preparation for TIRF microscopy was performed as previously reported with minor modifications (Bunnell et al., 2003). In brief, 0.01% poly-L-lysine–pretreated glass coverslips were coated with 10 µg/ml αCD45 (cat. no. 304002; BioLegend) or αCD3 (317326; BioLegend) in PBS overnight at 4°C, or 2 h at 37°C. Jurkat cells were either transduced with TMEM16F-RFP lentivirus, or transfected with plasmids encoding indicated proteins by electroporation (Amaxa). Cells were then seeded on αCD45 or αCD3-coated coverslips containing imaging buffer (1.25 ml Hepes [1 M], 10 ml FBS, and 38.75 ml RPMI without phenol red) and placed in an open perfusion chamber with a humidified environment at 37°C, 5% CO_2 (20/20 Technology). When inhibitors were used, cells were pretreated with 1 µM nocodazole or 1 µM blebbistatin (Sigma-Aldrich) for 30 min, and then washed extensively before proceeding with TIRF. Unless otherwise indicated, images were taken every 2 s for 5 min. TIRF microscopy was done as previously reported (Cocucci et al., 2014). In brief, the software used to control the system was SlideBook V5.0 (Intelligent Imaging). Images were acquired using a MarianaTD system based on an Axiovert 200M microscope equipped with an Alpha Plan-Apo 100x objective (1.46 NA; ZEISS), a TIRF slider with manual angle and focus controls (ZEISS), and a spherical aberration correction system (Infinity Photo-Optical). The incidence angle of the excitation light on the coverslip was adjusted to generate an evanescent field with a penetration depth of 100–200 nm.

Jurkat–Raji conjugates and confocal microscopy

Raji cells were incubated for 2 h with 1 µg/ml of staphylococcal enterotoxin E (SEE; Toxin Technology) at 37°C. After extensive washing, 10^5 Raji cells were mixed with 10^5 Jurkat cells and plated onto poly-L-lysine-coated coverslips in 24-well plates, incubated for 30 min at 37°C, and then fixed with 2% paraformaldehyde (PFA). To determine the localization of TMEM16F, reporter (TMEM16F-RFP) or TCR-β were used to distinguish Jurkat from Raji cells. For immunofluorescence assays, samples were permeabilized with 0.1% Triton X-100, blocked with 10% FBS plus 2% goat serum in PBS, and stained for TCR-Vβ8 (cat. no. 555604; BD), followed by Alexa Fluor 555–conjugated goat anti–mouse IgG2b secondary antibody (A-21147; Life Technologies). All samples were mounted with ProLong Gold Antifade Mountant with DAPI (Life Technologies). Images were taken using a FV1000 confocal microscope with a water objective lens (UPlanAPO 60×; NA 1.20; Olympus). For 3D and z-axis image reconstruction, 20 confocal sections, 0.4 µm apart, were assembled using ImageJ/Fiji software (NIH).

Lentivirus production, titration, and transduction

Lentiviral vectors were purified using GenElute HP Plasmid kits (Sigma-Aldrich). For lentivirus production, 293T cells were seeded in 10-cm cell culture dishes. The next day, cells were transfected with a mixture of 45 µl TransIT-293 Transfection Reagent (Mirus), and 15-µg packaging plasmids. For shRNA, 7.5 µg pLKO-Thy1.1-shRNA hairpins, 6.75 µg PAX2, and 0.75 µg pCMV-VSVG were used for transfection. For TMEM16F-RFP, 12 µg pHAGE2 vector, 0.6 µg tat, 0.6 µg rev, 0.6 µg gag/pol, and 1.2 µg VSV-G were used for transfection. Lentivirus-containing supernatant was collected at 24, 48, and 72 h after transfection, passed through 0.45-µm filter (Millipore), and subsequently concentrated by ultracentrifugation at 17,000 rpm for 90 min. The virus pellet was dissolved in PBS.

Lentivirus stock was titrated on Jurkat cells using Thy1.1 (for shRNA) or human NGFR (for TMEM16F-RFP) as a reporter. In brief, 1.5×10^4 Jurkat cells were co-cultured with serial dilutions of virus stock for 48 h in round-bottom 96-well plates. Infection rate was determined by flow cytometry analysis for reporter expression. The concentration of lentivirus was calculated using the following formula: virus/ml = percent infection (90% = 0.9) × cell number (15,000) × 1,000/X µl (where X is volume of virus added). The titer of lentivirus stocks was on average 10^7–10^8 infection U/ml.

For transduction, target cells were infected with multiplicity of infection (MOI) 1 in the presence of 8 µg/ml polybrene (Sigma-Aldrich). To induce TMEM16F-RFP expression, 1 µg/ml doxycycline (Sigma-Aldrich) was added to culture medium 1 d before analysis. Transduction efficiency for lentivirus was >98% for all experiments.

RNA extraction and real-time PCR

Total RNA was extracted with TRIzol (Life Technologies) according to the manufacturer's instructions. High Capacity RNA-to-cDNA kit (Applied Biosystems) was used for reverse transcription of purified RNA. All of the gene transcripts were quantified by real-time PCR with SYBR Green

Published October 24, 2016

Master Mix (Bio-Rad Laboratories) and a 7300 Real-Time PCR System (Applied Biosystems). The relative fold induction was calculated by the $2^{-\Delta\Delta}$ cycle threshold (CT) method. The sequences of primers for real-time PCR are: human TMEM16F, forward, 5′-GAAGAACAAGCCCGACCAGA-3′; human TMEM16F, reverse, 5′-CCACCTGGGTCACAC TCTTC-3′; human GAPDH, forward, 5′-TGGGCTACA CTGAGCACCAG-3′; and human GAPDH, reverse, 5′-GGGTGTCGCTGTTGAAGTCA-3′.

LBPA staining

LBPA staining was performed as previously reported with minor modifications (Varma et al., 2006). In brief, Jurkat cells were stimulated on 10 µg/ml αCD45 or αCD3-coated coverslips for 5 min, and then fixed with 2% PFA for 30 min at room temperature. Cells were then blocked with 0.1% BSA for 30 min and stained with anti-LBPA antibody (cat. no. Z-PLBPA; Echelon Biosciences) at 4°C overnight in the presence of 0.05% saponin (Sigma-Aldrich), followed by Alexa Fluor 488–conjugated goat anti–mouse IgG1 secondary antibody (A-21121; Life Technologies). Samples were mounted in ProLong Gold Antifade Mountant with DAPI.

Transmission electron microscopy

For T cell stimulation, 2×10^6/ml Jurkat T cells were incubated with 10 µg/ml biotin-conjugated anti–human CD3ε antibody (BioLegend), followed by cross-linking with 20 µg/ml streptavidin (Cell Signaling Technology) for 10 min at 37°C. Stimulation was stopped by adding the same volume of 2× fixative (2.5% glutaraldehyde, 1.25% paraformaldehyde, and 0.03% picric acid in 0.1 M sodium cacodylate buffer, pH 7.4). Cells were spun down at 1,500 rpm for 5 min. The cell pellet was fixed for 2 h at room temperature in the fixative, washed in 0.1 M cacodylate buffer, and postfixed with 1% osmium tetroxide (OsO_4)/1.5% potassium ferrocyanide ($KFeCN_6$) for 1 h, washed in water, and incubated in 1% aqueous uranyl acetate for 1 h. Cells were subsequently dehydrated in grades of alcohol (10 min each; 50%, 70%, 90%, 2 × 10 min 100%). The samples were then put in propylene oxide for 1 h and infiltrated overnight in a 1:1 mixture of propylene oxide and TAAB epon (Marivac Canada Inc.). The next day, the samples were embedded in TAAB epon and polymerized at 60°C for 48 h. Ultrathin sections (60 nm) were cut on a Reichert Ultracut-S microtome (Leica), transferred onto copper grids, stained with lead citrate, and examined in a JEOL 1200EX transmission electron microscope (JEOL) or a Tecnai G2 Spirit BioTWIN (FEI). Images were recorded with an AMT 2k CCD camera.

Image processing

All images were processed using ImageJ/Fiji software. For tracking of TMEM16F reaching the IS, TMEM16F-positive spots were examined using the Trackmate plug-in on Fiji. The number of TMEM16F-positive spots was plotted using Prism 6.0. Quantifications of LBPA-positive vesicles, LAT-GFP, and SH2-ZAP70-mCherry were done similarly. Intensity of SH2-ZAP70-mCherry was determined using intensity versus time plug-in. For the co-localization of TMEM16F and Rab proteins, fluorescence intensity for each protein was measured on a line manually drawn along TMEM16F-positive vesicles, and values (pixel) were plotted. For Pearson's correlation analysis of the spatial relationship between TMEM16F and Rab proteins, six to seven movies (each has at least 300 frames) were used to determine the correlation coefficient (*r*) using the JACoP plug-in.

LCMV infection and virus titer

6–12-wk-old adult mice were i.v. infected with 4×10^6 pfu of LCMV clone 13 (a gift from J. Wherry, University of Pennsylvania, Philadelphia, PA). LCMV titer in serum and tissue homogenates was determined by focus assay. In brief, MC57G cells were cultured in the presence of serially diluted samples for 48 h. Cell monolayers were fixed with 10% formalin (Sigma-Aldrich) in PBS, permeabilized by 1% Triton X-100, and then stained with anti-LCMV antibody VL-4 (cat. no. BE0106-R005mg; Bio X Cell) and peroxidase-linked secondary antibody (Jackson ImmunoResearch Laboratories). Plates were developed with SIGMA FAST OPD tablet (Sigma-Aldrich) at room temperature for 15–30 min. The reaction was terminated by washing the plates five times with distilled water.

Peptides and tetramers

Peptides for LCMV antigens GP33 (KAVYNFATM), GP276 (SGVENPGGYCL), NP396 (FQPQNGQFI), and GP61 (GLNGPDIYKGVYQFKSVEFD) were purchased from AnaSpec. PE-conjugated $H2D^b$ GP33-KAVYNFATM and $I\text{-}A^b$ LCMV GP66-77 tetramers were provided by the NIH Tetramer Facility (Atlanta, GA).

In vivo BrdU incorporation

Mice were given 2 mg BrdU (Sigma-Aldrich) i.p. 20–24 h before tissue harvest and analysis. BrdU incorporation was evaluated by flow cytometry using the BrdU Flow kit (BD) following the manufacturer's instructions.

BM Chimera

BM was prepared from tibias and femurs of WT (CD45.1) and *TMEM16F*$^{-/-}$ mice (CD45.2). Recipient *Rag1*$^{-/-}$ mice were sublethally irradiated (450 rad) and reconstituted with either 3×10^6 WT or TMEM16F$^{-/-}$, or a 1:1 mixture of WT and *TMEM16F*$^{-/-}$ BM cells. Recipient mice were treated with 2 mg/ml neomycin (Sigma-Aldrich) in drinking water for 4 wk. 8–12 wk after BM transfer, mice were infected with 4×10^6 LCMV clone 13 i.v.

Statistical analyses

All data are presented as means and SEM. The statistical significance of differences was calculated by two-tailed Mann-Whitney test using Prism 6.0 (GraphPad Software). $P \leq 0.05$ was considered significant (*, $P < 0.05$; **, $P < 0.01$; ***, $P < 0.001$; ****, $P < 0.0001$).

Online supplemental material

Fig. S1 shows that TCR-induced calcium flux is independent of TMEM16F. Fig. S2 demonstrates normal T cell development in TMEM16F deficiency. Fig. S3 shows the T reg cell population in TMEM16F-KO and control mice during LCMV-C13 infection. Fig. S4 shows the expression of type I IFN in TMEM16F-KO and control mice during LCMV-C13 infection. Fig. S5 presents a mechanistic model. Video 1 shows dynamic recruitment of TMEM16F to the IS. Video 2 displays that disruption of microtubules, but not actin–myosin contractions, blocks the recruitment of TMEM16F to the IS. Video 3 illustrates that TMEM16F mainly resides in a Rab7-positive late endosomal compartment. Video 4 shows that TMEM16F is not localized in Rab5-positive early endosomes. Video 5 demonstrates that TMEM16F is not localized in Rab11-positive recycling endosomes. Video 6 illustrates sustained TCR phosphorylation in the absence of TMEM16F. Video 7 shows enhanced and sustained formation of LAT microclusters, indicating hyperactivation of T cells when TMEM16F is lacking.

ACKNOWLEDGMENTS

We thank L. Jan for providing TMEM16F antibody; N. Hacohen and T. Eisenhaure for help and advice on lentivirus production; K. Wucherpfennig and P. Zhou for providing pLKO-Thy1.1 lentiviral vector; S. Nagata for pMX-TMEM16F-RFP construct; L. Samelson for LAT-YFP vector; J. Wherry for LCMV clone 13; and W. Ebina and D. Rossi for pHAGE2-TRE lentiviral vector and helpful discussion. We thank M. Ericsson and L. Trakimas from the Electron Microscopy Facility at Harvard Medical School for electron microscopy technical support and instrumentation, M. Ocana from the Neurobiology Imaging Facility at Harvard (NINDS P30 Core Center Grant #NS072030). We thank the NIH tetramer facility for providing LCMV-specific tetramers.

This work was supported by National Institutes of Health grants R01 GM075252 (T. Kirchhausen) and R01 AI083426 (F. Winau).

The authors declare no competing financial interests.

Submitted: 28 April 2016
Accepted: 16 September 2016

REFERENCES

Benzing, C., J. Rossy, and K. Gaus. 2013. Do signalling endosomes play a role in T cell activation? *FEBS J.* 280:5164–5176. http://dx.doi.org/10.1111/febs.12427

Bevers, E.M., and P.L. Williamson. 2010. Phospholipid scramblase: an update. *FEBS Lett.* 584:2724–2730. http://dx.doi.org/10.1016/j.febslet.2010.03.020

Blackburn, S.D., H. Shin, G.J. Freeman, and E.J. Wherry. 2008. Selective expansion of a subset of exhausted CD8 T cells by alphaPD-L1 blockade. *Proc. Natl. Acad. Sci. USA.* 105:15016–15021. http://dx.doi.org/10.1073/pnas.0801497105

Brunner, J.D., N.K. Lim, S. Schenck, A. Duerst, and R. Dutzler. 2014. X-ray structure of a calcium-activated TMEM16 lipid scramblase. *Nature.* 516:207–212. http://dx.doi.org/10.1038/nature13984

Bunnell, S.C., V.A. Barr, C.L. Fuller, and L.E. Samelson. 2003. High-resolution multicolor imaging of dynamic signaling complexes in T cells stimulated by planar substrates. *Sci. STKE.* 2003:PL8.

Castoldi, E., P.W. Collins, P.L. Williamson, and E.M. Bevers. 2011. Compound heterozygosity for 2 novel TMEM16F mutations in a patient with Scott syndrome. *Blood.* 117:4399–4400. http://dx.doi.org/10.1182/blood-2011-01-332502

Cocucci, E., R. Gaudin, and T. Kirchhausen. 2014. Dynamin recruitment and membrane scission at the neck of a clathrin-coated pit. *Mol. Biol. Cell.* 25:3595–3609. http://dx.doi.org/10.1091/mbc.E14-07-1240

Ehlen, H.W., M. Chinenkova, M. Moser, H.M. Munter, Y. Krause, S. Gross, B. Brachvogel, M. Wuelling, U. Kornak, and A. Vortkamp. 2013. Inactivation of anoctamin-6/Tmem16f, a regulator of phosphatidylserine scrambling in osteoblasts, leads to decreased mineral deposition in skeletal tissues. *J. Bone Miner. Res.* 28:246–259. http://dx.doi.org/10.1002/jbmr.1751

Fortian, A., and A. Sorkin. 2014. Live-cell fluorescence imaging reveals high stoichiometry of Grb2 binding to the EGF receptor sustained during endocytosis. *J. Cell Sci.* 127:432–444. http://dx.doi.org/10.1242/jcs.137786

Gagnon, E., D.A. Schubert, S. Gordo, H.H. Chu, and K.W. Wucherpfennig. 2012. Local changes in lipid environment of TCR microclusters regulate membrane binding by the CD3ε cytoplasmic domain. *J. Exp. Med.* 209:2423–2439. http://dx.doi.org/10.1084/jem.20120790

Grakoui, A., S.K. Bromley, C. Sumen, M.M. Davis, A.S. Shaw, P.M. Allen, and M.L. Dustin. 1999. The immunological synapse: a molecular machine controlling T cell activation. *Science.* 285:221–227. http://dx.doi.org/10.1126/science.285.5425.221

Hailey, D.W., A.S. Rambold, P. Satpute-Krishnan, K. Mitra, R. Sougrat, P.K. Kim, and J. Lippincott-Schwartz. 2010. Mitochondria supply membranes for autophagosome biogenesis during starvation. *Cell.* 141:656–667. http://dx.doi.org/10.1016/j.cell.2010.04.009

Hankins, H.M., R.D. Baldridge, P. Xu, and T.R. Graham. 2015. Role of flippases, scramblases and transfer proteins in phosphatidylserine subcellular distribution. *Traffic.* 16:35–47. http://dx.doi.org/10.1111/tra.12233

Hedrick, S.M., D.I. Cohen, E.A. Nielsen, and M.M. Davis. 1984. Isolation of cDNA clones encoding T cell-specific membrane-associated proteins. *Nature.* 308:149–153. http://dx.doi.org/10.1038/308149a0

Huang, B.X., M. Akbar, K. Kevala, and H.Y. Kim. 2011. Phosphatidylserine is a critical modulator for Akt activation. *J. Cell Biol.* 192:979–992. http://dx.doi.org/10.1083/jcb.201005100

Irannejad, R., N.G. Tsvetanova, B.T. Lobingier, and M. von Zastrow. 2015. Effects of endocytosis on receptor-mediated signaling. *Curr. Opin. Cell Biol.* 35:137–143. http://dx.doi.org/10.1016/j.ceb.2015.05.005

Kao, C., K.J. Oestreich, M.A. Paley, A. Crawford, J.M. Angelosanto, M.A. Ali, A.M. Intlekofer, J.M. Boss, S.L. Reiner, A.S. Weinmann, and E.J. Wherry. 2011. Transcription factor T-bet represses expression of the inhibitory receptor PD-1 and sustains virus-specific $CD8^+$ T cell responses during chronic infection. *Nat. Immunol.* 12:663–671. http://dx.doi.org/10.1038/ni.2046

Kobayashi, T., E. Stang, K.S. Fang, P. de Moerloose, R.G. Parton, and J. Gruenberg. 1998. A lipid associated with the antiphospholipid syndrome regulates endosome structure and function. *Nature.* 392:193–197. http://dx.doi.org/10.1038/32440

Lee, S.H., X.W. Meng, K.S. Flatten, D.A. Loegering, and S.H. Kaufmann. 2013. Phosphatidylserine exposure during apoptosis reflects bidirectional trafficking between plasma membrane and cytoplasm. *Cell Death Differ.* 20:64–76. http://dx.doi.org/10.1038/cdd.2012.93

Le Floc'h, A., Y. Tanaka, N.S. Bantilan, G. Voisinne, G. Altan-Bonnet, Y. Fukui, and M. Huse. 2013. Annular PIP3 accumulation controls actin architecture and modulates cytotoxicity at the immunological synapse. *J. Exp. Med.* 210:2721–2737. http://dx.doi.org/10.1084/jem.20131324

Malvezzi, M., M. Chalat, R. Janjusevic, A. Picollo, H. Terashima, A.K. Menon, and A. Accardi. 2013. Ca2+-dependent phospholipid scrambling by a reconstituted TMEM16 ion channel. *Nat. Commun.* 4:2367. http://dx.doi.org/10.1038/ncomms3367

Matsuo, H., J. Chevallier, N. Mayran, I. Le Blanc, C. Ferguson, J. Fauré, N.S. Blanc, S. Matile, J. Dubochet, R. Sadoul, et al. 2004. Role of LBPA and

Alix in multivesicular liposome formation and endosome organization. *Science.* 303:531–534. http://dx.doi.org/10.1126/science.1092425

Melowic, H.R., R.V. Stahelin, N.R. Blatner, W. Tian, K. Hayashi, A. Altman, and W. Cho. 2007. Mechanism of diacylglycerol-induced membrane targeting and activation of protein kinase Ctheta. *J. Biol. Chem.* 282:21467–21476. http://dx.doi.org/10.1074/jbc.M700119200

Monks, C.R., B.A. Freiberg, H. Kupfer, N. Sciaky, and A. Kupfer. 1998. Three-dimensional segregation of supramolecular activation clusters in T cells. *Nature.* 395:82–86. http://dx.doi.org/10.1038/25764

Ou, R., M. Zhang, L. Huang, and D. Moskophidis. 2008. Control of virus-specific $CD8^+$ T-cell exhaustion and immune-mediated pathology by E3 ubiquitin ligase Cbl-b during chronic viral infection. *J. Virol.* 82:3353–3368. http://dx.doi.org/10.1128/JVI.01350-07

Ousingsawat, J., P. Wanitchakool, A. Kmit, A.M. Romao, W. Jantarajit, R. Schreiber, and K. Kunzelmann. 2015. Anoctamin 6 mediates effects essential for innate immunity downstream of P2X7 receptors in macrophages. *Nat. Commun.* 6:6245. http://dx.doi.org/10.1038/ncomms7245

Paley, M.A., D.C. Kroy, P.M. Odorizzi, J.B. Johnnidis, D.V. Dolfi, B.E. Barnett, E.K. Bikoff, E.J. Robertson, G.M. Lauer, S.L. Reiner, and E.J. Wherry. 2012. Progenitor and terminal subsets of $CD8^+$ T cells cooperate to contain chronic viral infection. *Science.* 338:1220–1225. http://dx.doi.org/10.1126/science.1229620

Pálfy, M., A. Reményi, and T. Korcsmáros. 2012. Endosomal crosstalk: meeting points for signaling pathways. *Trends Cell Biol.* 22:447–456. http://dx.doi.org/10.1016/j.tcb.2012.06.004

Segawa, K., S. Kurata, Y. Yanagihashi, T.R. Brummelkamp, F. Matsuda, and S. Nagata. 2014. Caspase-mediated cleavage of phospholipid flippase for apoptotic phosphatidylserine exposure. *Science.* 344:1164–1168. http://dx.doi.org/10.1126/science.1252809

Smith-Garvin, J.E., G.A. Koretzky, and M.S. Jordan. 2009. T cell activation. *Annu. Rev. Immunol.* 27:591–619. http://dx.doi.org/10.1146/annurev.immunol.021908.132706

Stachowiak, J.C., F.M. Brodsky, and E.A. Miller. 2013. A cost-benefit analysis of the physical mechanisms of membrane curvature. *Nat. Cell Biol.* 15:1019–1027. http://dx.doi.org/10.1038/ncb2832

Staron, M.M., S.M. Gray, H.D. Marshall, I.A. Parish, J.H. Chen, C.J. Perry, G. Cui, M.O. Li, and S.M. Kaech. 2014. The transcription factor FoxO1 sustains expression of the inhibitory receptor PD-1 and survival of antiviral $CD8^+$ T cells during chronic infection. *Immunity.* 41:802–814. http://dx.doi.org/10.1016/j.immuni.2014.10.013

Suzuki, J., M. Umeda, P.J. Sims, and S. Nagata. 2010. Calcium-dependent phospholipid scrambling by TMEM16F. *Nature.* 468:834–838. http://dx.doi.org/10.1038/nature09583

Trajkovic, K., C. Hsu, S. Chiantia, L. Rajendran, D. Wenzel, F. Wieland, P. Schwille, B. Brügger, and M. Simons. 2008. Ceramide triggers budding of exosome vesicles into multivesicular endosomes. *Science.* 319:1244–1247. http://dx.doi.org/10.1126/science.1153124

Vardhana, S., K. Choudhuri, R. Varma, and M.L. Dustin. 2010. Essential role of ubiquitin and TSG101 protein in formation and function of the central supramolecular activation cluster. *Immunity.* 32:531–540. http://dx.doi.org/10.1016/j.immuni.2010.04.005

Varma, R., G. Campi, T. Yokosuka, T. Saito, and M.L. Dustin. 2006. T cell receptor-proximal signals are sustained in peripheral microclusters and terminated in the central supramolecular activation cluster. *Immunity.* 25:117–127. http://dx.doi.org/10.1016/j.immuni.2006.04.010

Vogel, G.F., H.L. Ebner, M.E. de Araujo, T. Schmiedinger, O. Eiter, H. Pircher, K. Gutleben, B. Witting, D. Teis, L.A. Huber, and M.W. Hess. 2015. Ultrastructural morphometry points to a new role for LAMTOR2 in regulating the endo/lysosomal system. *Traffic.* 16:617–634. http://dx.doi.org/10.1111/tra.12271

Weiss, H.J., W.J. Vicic, B.A. Lages, and J. Rogers. 1979. Isolated deficiency of platelet procoagulant activity. *Am. J. Med.* 67:206–213. http://dx.doi.org/10.1016/0002-9343(79)90392-9

Wherry, E.J. 2011. T cell exhaustion. *Nat. Immunol.* 12:492–499. http://dx.doi.org/10.1038/ni.2035

Willinger, T., M. Staron, S.M. Ferguson, P. De Camilli, and R.A. Flavell. 2015. Dynamin 2-dependent endocytosis sustains T-cell receptor signaling and drives metabolic reprogramming in T lymphocytes. *Proc. Natl. Acad. Sci. USA.* 112:4423–4428. http://dx.doi.org/10.1073/pnas.1504279112

Wollert, T., C. Wunder, J. Lippincott-Schwartz, and J.H. Hurley. 2009. Membrane scission by the ESCRT-III complex. *Nature.* 458:172–177. http://dx.doi.org/10.1038/nature07836

Xu, C., E. Gagnon, M.E. Call, J.R. Schnell, C.D. Schwieters, C.V. Carman, J.J. Chou, and K.W. Wucherpfennig. 2008. Regulation of T cell receptor activation by dynamic membrane binding of the CD3epsilon cytoplasmic tyrosine-based motif. *Cell.* 135:702–713. http://dx.doi.org/10.1016/j.cell.2008.09.044

Xu, P., R.D. Baldridge, R.J. Chi, C.G. Burd, and T.R. Graham. 2013. Phosphatidylserine flipping enhances membrane curvature and negative charge required for vesicular transport. *J. Cell Biol.* 202:875–886. http://dx.doi.org/10.1083/jcb.201305094

Yanagi, Y., Y. Yoshikai, K. Leggett, S.P. Clark, I. Aleksander, and T.W. Mak. 1984. A human T cell-specific cDNA clone encodes a protein having extensive homology to immunoglobulin chains. *Nature.* 308:145–149. http://dx.doi.org/10.1038/308145a0

Yang, H., A. Kim, T. David, D. Palmer, T. Jin, J. Tien, F. Huang, T. Cheng, S.R. Coughlin, Y.N. Jan, and L.Y. Jan. 2012. TMEM16F forms a $Ca2^+$-activated cation channel required for lipid scrambling in platelets during blood coagulation. *Cell.* 151:111–122. http://dx.doi.org/10.1016/j.cell.2012.07.036

Yudushkin, I.A., and R.D. Vale. 2010. Imaging T-cell receptor activation reveals accumulation of tyrosine-phosphorylated CD3ζ in the endosomal compartment. *Proc. Natl. Acad. Sci. USA.* 107:22128–22133. http://dx.doi.org/10.1073/pnas.1016388108

Zhang, N., and M.J. Bevan. 2011. $CD8^+$ T cells: foot soldiers of the immune system. *Immunity.* 35:161–168. http://dx.doi.org/10.1016/j.immuni.2011.07.010

Zhang, H., S.P. Cordoba, O. Dushek, and P.A. van der Merwe. 2011. Basic residues in the T-cell receptor ζ cytoplasmic domain mediate membrane association and modulate signaling. *Proc. Natl. Acad. Sci. USA.* 108:19323–19328. http://dx.doi.org/10.1073/pnas.1108052108

SUPPLEMENTAL MATERIAL

Hu et al., http://dx.doi.org/10.1084/jem.20160612

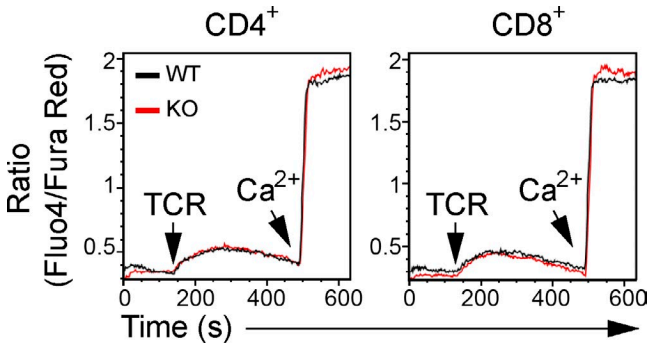

Figure S1. **TCR-induced calcium flux is independent of TMEM16F.** WT or TMEM16F-KO (KO) splenocytes were stained with Ca^{2+} indicator dyes Fura Red and Fluo-4 before stimulation by cross-linked anti-CD3 (5 µg/ml) at the indicated time (marked by arrows, TCR), followed by CaCl2 (marked by arrows, Ca^{2+}). Intracellular Ca^{2+} amounts are shown as a median ratio of Fluo-4/Fura Red over time.

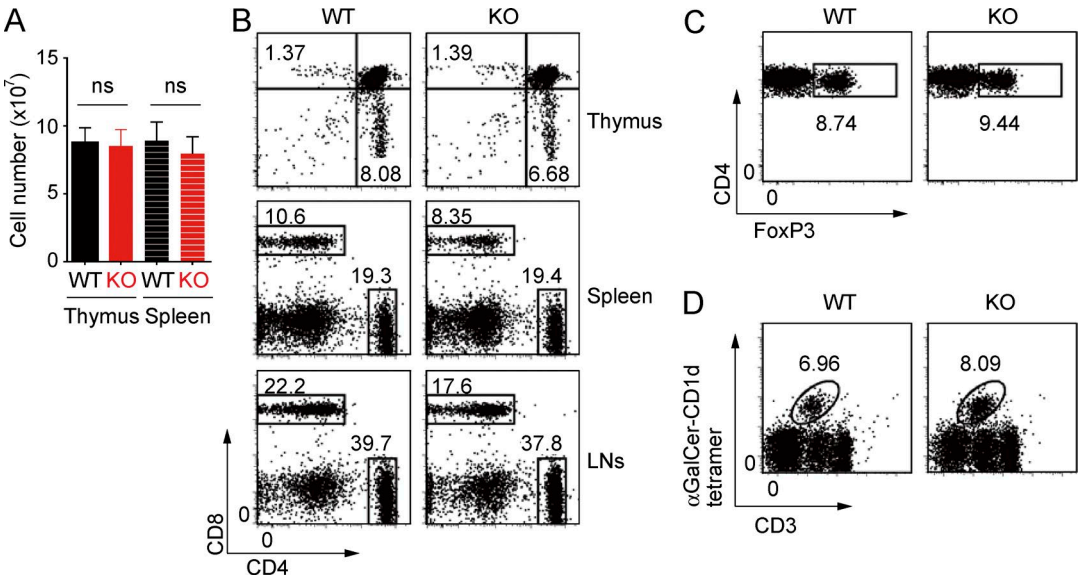

Figure S2. **Normal T cell development in TMEM16F-KO mice.** (A) Total lymphocyte numbers of thymus and spleen from WT or TMEM16F-KO mice. Results are displayed as mean ± SEM. (B–D) Frequencies of conventional T cells in thymus, spleen, and lymph nodes (LNs; B), T reg cells in spleen (C), and liver invariant NKT cells (D) assessed by flow cytometry. Data are representative of two to four independent experiments (n = 4–5 mice per group). Student's t test was used. ns, not significant.

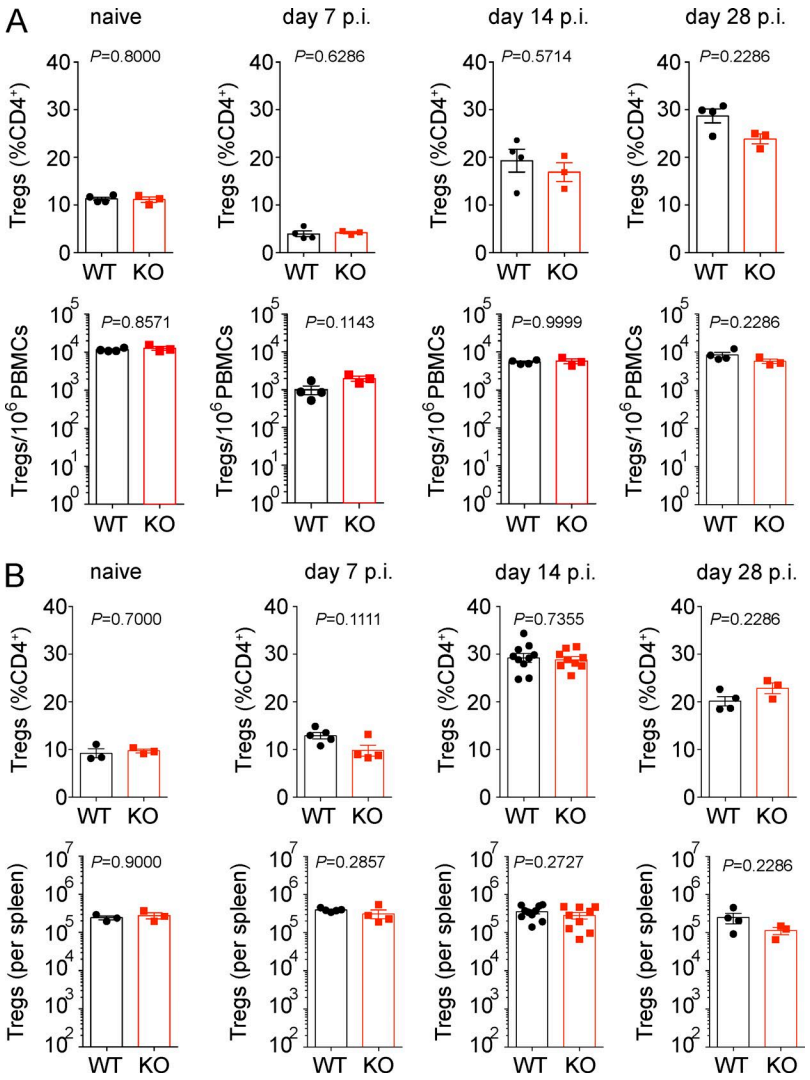

Figure S3. **T reg cell population in TMEM16F-KO and control mice during LCMV-C13 infection.** Flow cytometry analysis of T reg cells (FoxP3$^+$) in PBMCs (A) or splenocytes (B) from TMEM16F-KO or WT mice at indicated time points after LCMV-C13 infection. Frequencies (A and B, top row) and absolute cell number (A and B, bottom row) of T reg cells are shown. Data are representative of two to four independent experiments (n = 3–10 mice per group). Mann–Whitney U test was used.

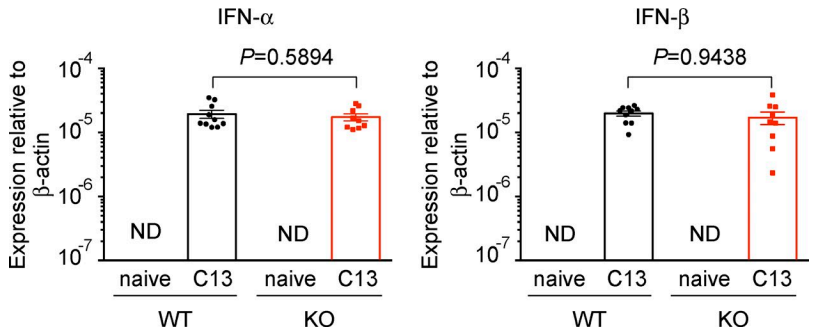

Figure S4. **Expression of type I IFN in TMEM16F-KO and control mice during LCMV-C13 infection.** mRNA level of IFN-α (left) and IFN-β (right) in spleen from LCMV-C13–infected mice (day 14 after infection) was determined by real-time PCR. Relative expression of IFN-α (left) or IFN-β (right) to β-actin was plotted. CT (threshold cycle) for IFN-α and IFN-β was measured between 28 and 31. *n* = 10 for WT and *n* = 9 for KO. No signal was detected in samples from naive mice after 40 cycles of amplification. ND, not detectable. P-value was determined by Mann–Whitney *U* test.

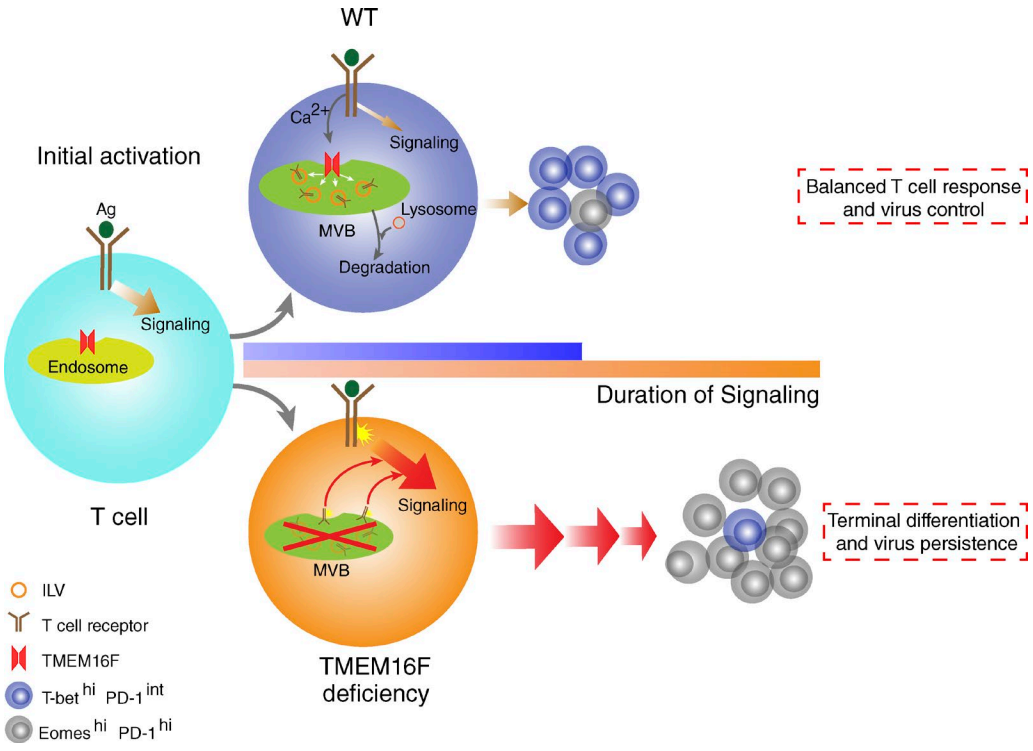

Figure S5. **Mechanistic model.** (top) TCR engagement, via increased intracellular Ca^{2+} levels, activates scramblase TMEM16F in late endosomes to mediate the formation of MVBs. Newly generated MVBs sequester intracellular TCR signaling complexes for subsequent lysosomal degradation to terminate T cell activation. This TMEM16F-mediated checkpoint determines the duration of signaling and the proper ratio of T-bet^{hi} to Eomes^{hi} effector T cells to facilitate virus clearance. (bottom) In the absence of TMEM16F, generation of MVBs is hampered, TCR signaling molecules accumulate, and T cell activation is sustained. Breaking the TMEM16F checkpoint leads to prolonged signaling that shifts the balance toward terminally differentiated Eomes^{hi} T cells and ultimate loss of virus protection.

Video 1. **Dynamic recruitment of TMEM16F to the IS.** Live imaging of Jurkat cells expressing TMEM16F-RFP by TIRF microscopy shows the dynamic recruitment of TMEM16F to the IS upon antigen stimulation. Cells were stimulated on 10 µg/ml αCD3-coated coverslips. Images were taken at the rate of one frame per 2 s for 348 s. Red, TMEM16F.

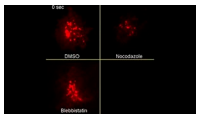

Video 2. **Disruption of microtubules, but not actin–myosin contractions, blocks the recruitment of TMEM16F to the IS.** TIRF live imaging of Jurkat cells pretreated with vehicle (DMSO, top left), 1 µM nocodazole (top right), or 1 µM blebbistatin (bottom left) before stimulation on 10 µg/ml αCD3-coated coverslips demonstrates that movement of TMEM16F-RFP toward the IS depends on microtubules but not actin. Images were taken at the rate of one frame per 0.5 s for 149 s. Red, TMEM16F.

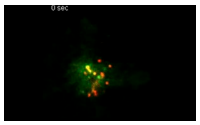

Video 3. **TMEM16F mainly resides in a Rab7-positive late endosomal compartment.** Dynamic movements of TMEM16F and Rab7 at the IS reveal that TMEM16F mainly resides in a Rab7-positive late endosomal compartment. TIRF live images of Jurkat cells overexpressing TMEM16F-RFP and Rab7-GFP placed on 10 µg/ml αCD3-coated coverslips were taken at the rate of one frame per 0.5 s for 150 s. Pearson's coefficient, 0.727. Red, TMEM16F; green, Rab7.

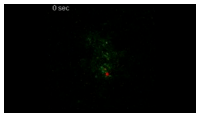

Video 4. **TMEM16F is not localized in Rab5-positive early endosomes.** Dynamic movements of TMEM16F and Rab5 at the IS reveal that TMEM16F is not spatially correlated with Rab5. TIRF live images of Jurkat cells overexpressing TMEM16F-RFP and Rab5-GFP placed on 10 µg/ml αCD3-coated coverslips were taken at the rate of one frame per 0.5 s for 150 s. Pearson's coefficient, 0.186. Red, TMEM16F; green, Rab5.

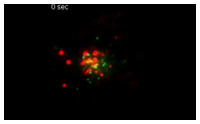

Video 5. **TMEM16F is not localized in Rab11-positive recycling endosomes.** Dynamic movements of TMEM16F and Rab11 at the IS reveal that TMEM16F is not spatially correlated with Rab11. TIRF live images of Jurkat cells overexpressing TMEM16F-RFP and Rab11-GFP placed on 10 µg/ml αCD3-coated coverslips were taken at the rate of one frame per 0.5 s for 149 s. Pearson's coefficient, 0.217. Red, TMEM16F; green, Rab11.

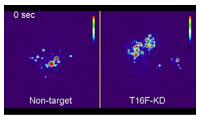

Video 6. **Sustained TCR phosphorylation in the absence of TMEM16F.** Tracking of phosphorylated TCRs using a live-cell reporter (mCherry-tSH2 (ZAP70)) demonstrates that phosphorylation of TCR is sustained in the absence of TMEM16F (T16F-KD) when compared with control (nontarget). Jurkat cells overexpressing mCherry-tSH2 (ZAP70) were stimulated on 10 µg/ml αCD3-coated coverslips. Images were taken by TIRF microscopy at the rate of one frame per 2 s for 300 s. Heat map of mCherry-tSH2 intensity is shown. Red, mCherry-tSH2.

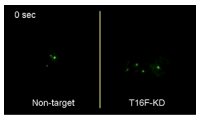

Video 7. **Enhanced and sustained formation of LAT microclusters shows hyperactivation of T cells when TMEM16F is lacking.** Dynamics of LAT microclusters in activated Jurkat cells were monitored by TIRF microscopy. Jurkat cells overexpressing LAT-YFP were stimulated on 10 µg/ml αCD3-coated coverslips. Images were taken by TIRF microscopy at the rate of one frame per 5 s for 360 s. Green, LAT.